PERFORMANCE OPTIMIZATION ON AXIAL-FLUX PERMANENT MAGNET CORELESS GENERATOR USING NOVEL HYBRID COMPUTATIONAL METHOD BASED ON GENETIC ALGORITHM AND PATTERN SEARCH

LOK CHOON LONG

FACULTY OF SCIENCE
UNIVERSITY OF MALAYA
KUALA LUMPUR

2016

PERFORMANCE OPTIMIZATION ON AXIAL-FLUX PERMANENT MAGNET CORELESS GENERATOR USING NOVEL HYBRID COMPUTATIONAL METHOD BASED ON GENETIC ALGORITHM AND PATTERN SEARCH

LOK CHOON LONG

DISSERTATION SUBMITTED IN FULFILMENT OF THE REQUIREMENTS FOR THE DEGREE OF MASTER OF SCIENCE

FACULTY OF SCIENCE
UNIVERSITY OF MALAYA
KUALA LUMPUR

2016

UNIVERSITY OF MALAYA

ORIGINAL LITERARY WORK DECLARATION

Name of Candidate: LOK CHOON LONG

Registration/Matric No: SGR 130 119

Name of Degree: MASTER`S DEGREE OF SCIENCE

Title of Project Paper/Research Report/Dissertation/Thesis ("this Work"):

PERFORMANCE OPTIMIZATION ON AXIAL-FLUX PERMANENT MAGNET CORELESS GENERATOR USING NOVEL HYBRID COMPUTATIONAL METHOD BASED ON GENETIC ALGORITHM AND PATTERN SEARCH

Field of Study: EXPERIMENTAL PHYSICS

I do solemnly and sincerely declare that:

(1) I am the sole author/writer of this Work;
(2) This work is original;
(3) Any use of any work in which copyright exists was done by way of fair dealing and for permitted purposes and any excerpt or extract from, or reference to or reproduction of any copyright work has been disclosed expressly and sufficiently and the title of the Work and its authorship have been acknowledged in this Work;
(4) I do not have any actual knowledge nor do I ought reasonably to know that the making of this work constitutes an infringement of any copyright work;
(5) I hereby assign all and every rights in the copyright to this Work to the University of Malaya ("UM"), who henceforth shall be owner of the copyright in this Work and that any reproduction or use in any form or by any means whatsoever is prohibited without the written consent of UM having been first had and obtained;
(6) I am fully aware that if in the course of making this Work I have infringed any copyright whether intentionally or otherwise, I may be subject to legal action or any other action as may be determined by UM.

Candidate's Signature Date:

Subscribed and solemnly declared before,

Witness's Signature Date:

Name:

Designation:

ABSTRACT

Complex real-world problems can be solved by heuristic optimization efficiently. Improved hybrid optimization method using Pattern Search (PS) and Genetic Algorithm (GA) onto Axial-Flux Permanent Magnet (AFPM) Coreless generator is presented in this thesis, and the optimization is based on the popular multi-objective sizing equation. This hybrid model utilizes concepts from GA and invents new generation chromosomes not only through mutation and crossover operation but also by mechanism of PS. In the design procedure, hybrid optimization model with some predefined constraints for the objective function have been taken into consideration which include the physical limitations and performance characteristics. The dimensions of the machine optimized with multiple adjustments to the number of magnet pole, the number of winding turns and air-gap distance in order to gain the highest power density within desired dimensional constraints. By using the proposed hybrid optimization method, the objective function has obtained a more accurate maximum power density with the least execution time over population compared with GA and PS. In addition, electromagnetic field and electromagnetic characteristics of the chosen generator is subject to Finite-Element Analysis (FEA). A finalized low power Axial-flux permanent magnet (AFPM) generator is fabricated, examined and testified to produce desired output. It has been observed that the experiment result agreed with the simulation result.

ABSTRAK

Masalah dunia yang komplek dapat diselesaikan menggunakan pengoptimuman teknik heuristik dengan berkesan. Tesis ini membentangkan hibrid Algoritma Genetik (GA) dan "Pattern Search (PS)" ke atas penjana kuasa paksi fluks segerak magnet kekal (AFPM) tanpa teras, optimasi ini dijalankan berdasarkan formula size persamaan. Model hibrid ini menggunakan konsep di mana Algoritma Genetik menghasilkan generasi kromosom daripada proses mutasi dan proses tindihan. Selain itu, mekanisma "Pattern Search" juga diguna-sama dalam operasi hibrid tersebut. Dalam merekabentuk fungsi objectif prototaip ini, model hibrid bersertakan ciri kekangan yang ditetapkan turut mempertimbangkan pelbagai ciri praktikal mesin seperti had fizikal dan ciri-ciri prestasi mesin. Ciri-ciri dimensi mesin yang didapati melalui pengoptimuman seperti bilangan kutub magnet, bilangan lilitan dalam stator, jarak antaran untuk mencapai kepadatan kuasa maksimum berjaya didapatkan. Dengan menggunakan model hibrid ini, ia dapat mengira kepadatan kuasa maksimum dalam masa tersingkat yang lebih efisien daripada model GA dan PS. Daya electromagnet dan sifat elektromagnetik mesin juga dioptimumkan melalui analisi unsur terhingga. Oleh itu, rekabentuk komprehensif penjana kuasa yang disimpulkan dibina dan diuji sehingga mencapai keputusan yang diinginkan. Ia juga didapati bahawa keputusan eksperimen sama dengan keputusan simulasi.

ACKNOWLEDGEMENTS

I would like to thank my supervisors, Prof. Dr. Ramesh Subramaniam, and Dr. Vengadaesvaran Balakrishnan for their vital advice and encouragement. Without their guidance and support, this research would not have been possible. Moreover, I offer my regards and blessings to all my friends, classmates, labmates and neighbours who supported me in any respect during the completion of this project. My special appreciation and recommendation also goes to my beloved parents for their kindness, patients and understanding as well as their good advice towards this study. May God bless all of them.

This work was supported by the University of Malaya research grants from IPPP (UMRG) PG127-2014B for Master`s Degree.

TABLE OF CONTENTS

Abstract…… iii

Abstrak…….. iv

Acknowledgements v

Table of Contents vi

List of Figures ix

List of Tables xii

List of Symbols and Abbreviations xiii

CHAPTER 1: INTRODUCTION 1

1.1 Introduction 1

1.2 Research Objectives 5

1.3 Scope of Project 6

1.4 Thesis Outlines 6

CHAPTER 2: LITERATURE REVIEW 8

2.1 Introduction 8

2.2 Types of Axial-Flux Permanent Magnet Machine 10

2.2.1 Single-Rotor Single-Stator Structure 10

2.2.2 Double-Rotor Single-Stator Structure 11

2.2.3 Single-Rotor Double-Stator Structure 14

2.2.4 Multi-Rotor Multi-Stator Structure 16

2.3 Analysis of Axial-Flux Permanent Magnet Machine 17

2.3.1 Electromagnetic Field Analysis 17

2.3.2 Torque Analysis 20

2.4 Design Procedure of the AFPM Machines 21

2.5 Applications of AFPM Machines 23

CHAPTER 3: THEORY OF AXIAL-FLUX PERMANENT MAGNET MACHINES 24

3.1 Introduction 24

3.2 Basic Equations 24

3.2.1 Torque 24

3.2.2 Back-EMF and Power 29

3.2.3 Rotating Permanent Magnets 31

3.3 Design Variations 34

3.3.1 Permanent-Magnet Span 34

3.3.2 Winding Factors 34

3.3.3 Number of Stator Slots 36

3.3.4 Winding Configurations 37

CHAPTER 4: DESIGN OPTIMIZATION, METHODOLOGY AND ANALYSIS 39

4.1 Introduction 39

4.2 Design Procedure 40

4.3 Sizing Equations 41

4.4 Losses and Efficiency 45

4.5 Fitness Function 46

4.6 Genetic Algorithm (GA) 47

4.6.1 Chromosome 47

4.6.2 Crossover 48

4.6.3 Mutation 49

4.7 Pattern Search Tool (PS) 49

4.8 Hybrid GA-PS Algorithm 50
4.9 Finite Element Analysis (FEA) 56
4.10 Final Designs 59
4.11 Machine Construction 61
4.11.1 Stator 62
4.11.2 Winding the Stator 62
4.11.3 Rotor 63
4.11.4 Permanent Magnet 65
4.12 Experiment Setup 65

CHAPTER 5: RESULTS AND DISCUSSION 68

5.1 Introduction 68
5.2 Optimization Results 68
5.3 Simulation Results 70
5.3.1 Back-EMF Waveform 71
5.3.2 Eddy Current Losses 72
5.3.3 Cogging Torque 73
5.4 Experiment Results 74
5.4.1 Back-EMF Measurement 74
5.4.2 Load Test Measurement 75
5.4.3 Cogging Torque 76
5.4.4 Efficiency 77

CHAPTER 6: CONCLUSION 80

References 82
List of Publications and Papers Presented 91

LIST OF FIGURES

Figure 2.1: (a) Single-sided AFPM machine. (b) Cross-section of AFPM magnetic flux path. 11

Figure 2.2: (a) Double-sided AFPM machine. (b) "TORUS" type AFPM machine 12

Figure 2.3: (a) North-North magnet arrangement. (b) North-South magnet arrangement 13

Figure 2.4: (a) Double-stator single-rotor AFPM machine. (b) Single-rotor double-stators "TORUS" structure. 14

Figure 2.5: (a) Surface-mounted permanent magnet rotor disc. (b) Buried permanent magnet in a rotor core 15

Figure 2.6: (a) Air-core multistage AFPM machine. (b) Multistage structure; triple-stator double rotor 16

Figure 2.7: Flux density in a 2D FEA of a radial-flux PM machine. 18

Figure 2.8: (a) 3D auto-mesh generation. (b) Flux-density plot 19

Figure 2.9: 3D FEA and analytical model comparison for cogging torque 21

Figure 3.1: Torque production vector in an axial-flux machines 25

Figure 3.2: Sinusoidal distributed conductors of one phase on the stator pole section ..25

Figure 3.3: Air-gap flux density in a cross-section of the surface-mounted AFPM machine. 31

Figure 3.4: Flux density distribution of a sinusoidal current sheet and a rectangular magnet 33

Figure 3.5: Stator winding configurations for 3, 6, 9, 12, 15, 18 slots 37

Figure 4.1: Typical prototype waveform factor 41

Figure 4.2: Flowchart of GA-PS optimization 50

Figure 4.3: GA-PS optimizer developed in MATLAB GUI 53

Figure 4.4: Rosenbrock`s wave function 54

Figure 4.5: Rosenbrock`s test function by Patterm Search 54
Figure 4.6: Rosenbrock`s test function by Genetic Algorithm 55
Figure 4.7: Rosenbrock`s test function by Hybrid GA-PS 55
Figure 4.8: Meshed model for one-fourth of the AFPM machine 57
Figure 4.9: Magnetic flux vector distribution obtained by FEA 57
Figure 4.10: CAD design and FEA flux density of the 1/4 model 58
Figure 4.11: Coil windings with iron-stator core (center) 58
Figure 4.12: Proposed AFPM generator based on design data. 60
Figure 4.13: Prototype three-phase AFPM machine 61
Figure 4.14: Coil winding on stator back plate 62
Figure 4.15: Individual stator coil winding 63
Figure 4.16: Windings configuration for 12-stator core count 63
Figure 4.17: Eight-pole single-rotor double-stator assembly 64
Figure 4.18: Rotor disc with 8 permanent magnets. 64
Figure 4.19: Variety of magnets used in permanent magnet machine 65
Figure 4.20: Hardware setup of experiment test bench 66
Figure 4.21: Hardware schematics of prototype generator.. 66
Figure 5.1: (a) Fitness value versus population. (b) Maximum constraint versus population. (c) Execution time versus population 69
Figure 5.2: Field analysis of three dimensional auto-mesh generation 71
Figure 5.3: Magnetic flux density distribution of the air gap for average radius 71
Figure 5.4: back-EMF in FEA 72
Figure 5.5: No-load losses versus speed 73
Figure 5.6: Cogging torque between the iron-stator core and air-core stator of AFPM generator 74
Figure 5.7: Measured back-EMF waveform of the AFPM prototype 75

Figure 5.8: No load back-EMF versus speed 75

Figure 5.9: Output power versus speed 76

Figure 5.10: Torque versus speed 77

Figure 5.11: Efficiency versus speed 78

Figure 5.12: Temperature versus speed 78

LIST OF TABLES

Table 3.1: Slot numbers and the corresponding number of slots per pole per phase 36

Table 3.2: Various configuration of winding pitch and the number of slots in each pole, per phase 38

Table 4.1: Design restriction and requirements 52

Table 4.2: Design data of proposed machine 60

LIST OF SYMBOLS AND ABBREVIATIONS

A	:	Electrical Loading
ABS	:	Acrylonitrile Butadiene Styrene
AC	:	Alternating Current
AFIR	:	Axial-Flux Internal Rotor
AFIPM	:	Axial-Flux Interior Rotor Permanent Magnet
AFPM	:	Axial-Flux Permanent Magnet
AFPMG	:	Axial-Flux Permanent Magnet Generator
Bg	:	Magnetic flux density [Tesla]
CAD	:	Computer Aided Design
CNC	:	Computer Numerical Control
DAQ	:	Data Acquisition Unit
DC	:	Direct Current
EMF	:	Electro Motive Force
Freq	:	Frequency
FE	:	Finite Element
FEA	:	Finite Element Analysis
FEM	:	Finite Element Method
GA	:	Genetic Algorithm
GA-PS	:	Genetic Algorithm-Pattern Search
GFA	:	Genetic-Fuzzy Algorithm
GUI	:	Graphic User Interface
Hz	:	Hertz
IR	:	Infrared
MATLAB	:	MATrix LABoratory (TradeMark)
mm	:	millimeter
mT	:	milli Tesla
NdFeB	:	Neodymium-iron-boron
NIB	:	Neodymium-iron-boron
Nm	:	NewtonMeter
NN	:	North-North

NS	:	North-South
Ohm	:	Ohm Resistance
PM	:	Permanent Magnet
PS	:	Pattern Search
PSO	:	Particle Search Optimization
RFPM	:	Radial-Flux Permanent Magnet
RMS	:	Root Mean Square
RPM	:	Rotation Per Minute
VFD	:	Variable Frequency Drive
W	:	Watt
2D	:	Two Dimensional
3D	:	Three Dimensional

CHAPTER 1: INTRODUCTION

1.1 Introduction

Over the years, various optimization techniques and software developed to improve electric machine design; one particularly powerful modern optimization tool is the Genetic Algorithm (GA). Genetic Algorithm has often been chosen for the machine optimization due to several advantages despite the objective for the optimization is not always the same, the reason is because the objectives vary with the application in which the machine is used. In year 1999, sizing equation was developed for the axial-flux machine optimization via shape modification (S Huang, Luo, Leonardi, & Lipo, 1997). Huang *et al.* also derived general sizing equation and power density equation for the radial-flux permanent magnet (RFPM) machines, the equation is a systematic method that compares the capabilities of various configurations performed in multi-objective optimization problem (Surong Huang, Luo, Leonardi, & Lipo, 1998; Parviainen, Niemela, & Pyrhonen, 2004; Qu & Lipo, 2003). Later, analysis of AFPM coreless generator was conducted by Virtic *et al*. using magnetic equivalent circuit, and the proposed method is lack of dimensional modification (Virtič & Avsec, 2011). Chung *et al*. presented 3D electromagnetic finite element analysis and basic structure adjustment, but only 4 parameters (output power density, machine`s efficiency, maximum current density and maximum rms phase voltage) were considered as optimization variables. Moreover, the optimization method used was the "Conjugate Gradient" which is not suitable to solve a non-linear multi-objective function (Chung & You, 2014). Mahmud *et al*. developed AFPM motor optimization using purely Genetic Algorithm in 2013 (Ali Mahmoudi, Kahourzade, Rahim, & Hew, 2013), a method that uses GA-based sizing equations to minimize the AFPM machine size with performance analysis in FEA. Although GA optimization method does not depend on the starting point of the function

searches as well as does not require detail information of the fitness function, the method also does not converge to the actual depth of the objective function thus giving less accurate optimization outputs (Rostami, Feyzi, Pyrhönen, Parviainen, & Behjat, 2012). Another weak point of the GA method is it requires substantial high amount of population to converge to the actual optimal point compared to hybrid optimization method. As a result, the design parameter obtained by Genetic Algorithm may not be that accurate.

Permanent magnet generators have been used for power generation many years dated back to almost 150 years ago (Hosseini, Agha-Mirsalim, & Mirzaei, 2008). Many manufacturers prefer direct-drive (no gear box) permanent magnet (PM) generators particularly in wind turbine technologies that favor the radial-flux generator type because it is suitable for high speed operation (Santiago & Bernhoff, 2010). However, axial-flux machines have recently become more important subject of study because of the decreasing cost of high-energy permanent magnet materials; the Neodymium-Iron-Boron (NdFeB) in particular. It has resulted in rapid permanent magnet generator development, especially for wind energy power applications. An axial–flux permanent magnet machine is the machine which produces magnetic flux in axial direction (Sharma, Bhatti, & Ramakrishnan, 2011). As known, the axial-flux permanent magnet machines have higher power density and higher driving torque (HÜNER & AKÜNER, 2012; Sadeghierad, Lesani, Monsef, & Darabi, 2009a) compared to induction machines, this type of generator has very simple and robust structure together with its` excellent electro-thermal properties (Rovio, Vihriälä, Söderlund, Kriikka, & Hyppönen, 2001). Because it can be designed with no stator core, an axial-flux permanent magnet (AFPM) generator with coreless stators are regarded as high-efficiency machines for power generation systems, a generator with this type of design can operate at higher efficiency than conventional induction generator. Besides, the high compactness and disc-shaped

profile make this type of machine particularly suitable for mechanical integration with wind turbines and internal combustion engines in narrow space.

Axial-flux permanent magnet (AFPM) generator has several unique advantages, the main unique feature in this study is the elimination of iron stator core, and thus the reluctance in the magnetic equivalent circuit is minimized. In an AFPM coreless generator, only little cogging torque exists within the air gap and it can be used with all small mechanical input designs (Bumby & Martin, 2005; HÜNER & AKÜNER, 2012). One limiting parameter in high-speed axial-flux generator is the magnet temperature, which it must be kept cold to be efficient (Sadeghierad et al., 2009a). Currently, there are many types of winding and magnet arrangements developed over these years but mostly are intended for wind turbine applications (Muljadi, Butterfield, & Wan, 1999a). Axial-flux permanent magnet (AFPM) generator is favored over wound-rotor generators due to it does not require any external excitation current which can significantly reduce the machine cost (Baptista, Kothandaraman, & Vijay, 2010). AFPM coreless generators are also eligible contenders for various power generation applications particularly in direct-drives over a wide operational speed range (Fei, Luk, & Jinupun, 2010). Compared to conventional generator with coupled gearbox, a direct-coupled generator system eliminates mechanical gear, hence reduces system size, minimizes components wear and lowers maintenance cost. In addition, this type of generator also responses to load variations and wind fluctuations more quickly. To meet higher power output, an axial-flux generator can be operated at high speed to substantially reduce in size and weight, because as rotor speed increases, the machine size decreases for a given output literally satisfies the Faraday`s Law of Induction (Kuo & Wieman, 2016).

Other advantages of AFPM generator is it can be in modular configuration for better cooling and can also be designed for larger output power (Jung & Cho, 2011). The surface-flux generator has higher power density than a traditional induction

generator (Muljadi et al., 1999a) for generating output power. Previous researches had shown that multilayer windings provide higher power density and easier stator construction (HÜNER & AKÜNER, 2012). However, for rotor operating at high speed, friction and windage in air gap can cause losses which result in efficiency drop and heat production (El Shahat, Keyhani, & El Shewy, 2010). In a large diameter rotor with large number of poles, it is ideal for low speed application (Virtič & Avsec, 2011). A recent comprehensive finding by Pop *et al.* shows that axial-flux generator has overall estimated costs lower than those radial-flux generator type designs mainly due to cheaper manufacturing cost (Dubois, Polinder, & Ferreira, 2000; Li & Chen, 2008). In machine application, AFPM motors and generators are particularly suitable for electrical vehicles, pumps, fans, valve controls, robots and industrial equipment (Mueller & McDonald, 2009).

In this research, hybrid GA-PS is used as the optimization method to optimize an AFPM coreless generator. To achieve that, geometrical and electrical parameters are considered to perceive this multi-objective problem in order to achieve maximum power density output and sinusoidal waveform. As opposed to GA algorithm, GA comprises parallel points to be searched in a population (Cao & Wu, 1999; Dao, Abhary, & Marian, 2016) while PS searches the minimum point left from the GA. In this method, the hybrid model mitigates GA-related problem such as slow convergence speed, easily fall into the partial optimum (Marinakis, Marinaki, & Dounias, 2010). The design optimization of a 120W, three-phase, 65Hz, four-pole pair AFPM coreless generator is based on the practical limitation for a typical small wind turbine generator. The design objectives are determined as with least cogging torque, and have maximum power density output with desired induced back-EMF waveform. 3D Finite Element Analysis (FEA) is used to compute the magnetic field of the AFPM generator, because FEA can produce more accurate results than the traditional analytical method, whose the

magnetic circuit is more complex in rotating machine design (De la Barriere, Hlioui, Ben Ahmed, Gabsi, & LoBue, 2012). The proposed generator development method is comprehensive for designing an arbitrary-parameter arbitrary-capacity double-stator single-rotor AFPM coreless generator. To verify the proposed generator, the designed AFPM coreless generator is fabricated and tested in test lab. It is found that the designed generator can meet the required specifications. Overall, the optimized AFPM coreless generator displays low cogging torque with desired output power density that comply to analytical results based on sizing equation and FEA results.

1.2 Research Objectives

In this research, improved optimization methods based on hybrid GA-PS and design methodology are developed for the double-sided AFPM coreless generator. The design optimization of 120W, 3-phase, 65Hz, 8-pole AFPM coreless generator uses hybrid GA-PS based on the machine sizing equation, desired requirements, and practical considerations. Minimization of machine size is performed considering various parameters such as the air-gap length, diameter ratio, air-gap flux density, winding turns, electrical loading, winding coefficient and stator-slot number. In short, the aims of the research are;

- To incorporate new GA-PS hybrid algorithm in optimizing AFPM generator.
- To develop optimization design procedure based on the derived equations for AFPM generator.
- To design an optimized AFPM generator with maximum power density, minimum cogging torque and machine losses.
- To evaluate the performance of the designed AFPM generator by comparing between simulated and experimental results.

1.3 Scope of Project

This research work is carried out to develop analytical and design methods to be part of iterative procedure for designing AFPM generator. The proposed design tool takes advantage of hybrid optimization such as the Genetic Algorithm (GA) and Pattern Search (PS) to obtain more accurate fitness value with the least computation time over population. Finite element analysis is used in the design process, the presented generator design has a minimum cogging torque, highest power density with sinusoidal back-EMF. The 120W, three-phase, 65Hz, 8-pole axial-flux permanent magnet coreless generator in this thesis uses hybrid GA-PS that depends on sizing equation. Various winding configurations and coil pitches are also explored to achieve the most sinusoidal back-EMF waveform. The performance of the proposed AFPM generator is verified in simulation through ANSYS Maxwell. It is observed that the designed AFPM generator can accommodate the design specifications. To validate the FEA simulation result of the proposed design, a standard prototype is built and evaluated with various experiments. It has been observed that the experiment result agreed with the simulation result.

1.4 Thesis Outlines

This thesis comprises **SIX** chapters as follows:

Chapter 1 contains the subject introduction, objectives and chapter overview.

Chapter 2 presents literature study and review on the axial-flux permanent magnet machine/generator.

Chapter 3 outlines the designing principles, theories, derivation, basic electrical and magnetic parameters of the axial-flux permanent magnet machine.

Chapter 4 presents all the methodology, to derive sizing equation and prototype fabrication for the AFPM generator. Hybrid GA-PS optimization is presented that

corresponds to the design restrictions, requirements, chromosome representation, crossover and mutation. Experiment setup is also presented.

Chapter 5 outlines the optimization results, simulation results and experiment results of the optimized AFPM coreless generator.

Chapter 6 is the summary which concludes the overall research project.

CHAPTER 2: LITERATURE REVIEW

2.1 Introduction

Applications of electric machines were dated back since the 1800s, and those available were only primitive Direct-Current (DC) permanent magnet machines (Duan & Ionel, 2013). At present, electrical machines that have dominated the markets are the radial-flux machines even though axial-flux machines had been introduced to market in the 70s and 80s (Campbell, 1975; Leung & Chan, 1980). Axial-flux machines were only much research interest particularly for special-purpose applications or due to limited geometrical considerations. As an alternative, axial-flux machines also exhibit high torque-to-weight ratio as well as better efficiency (M Aydin, Huang, & Lipo, 2004). AFPM machines have one unique feature; the machine efficiency can be improved significantly as the field excitation losses are eliminated, hence this reduces the rotor losses and higher power density can be achieved (Oh & Emadi, 2004). AFPM machines can be iron-core or air-core (coreless), double-sided or single-sided, single-staged or multi-staged and can be made of interior mounted or surface-mounted permanent magnet (C. Chan et al., 1996). Although there are many categories of permanent magnet generator available, only the AFPM generator is discussed here. Among many types of AFPM machine, the double-sided AFPM generator is widely studied and applied. The structure of double-sided AFPM machine has highest torque-to-volume ratio, particularly for machine with high number of pole pairs (Choi, Lee, Ko, & Jang, 2011). This type of generator has a simple and sturdy structure together with its` excellent electro-thermal properties (Rovio et al., 2001). The main advantage in this study is the elimination of iron core and thus the reluctance in the magnetic equivalent circuit is critically minimized. With no stator iron core, there are Eddy currents induced in the stator conductors due to rotating magnetic field flux from the permanent magnets

(Wang, Kamper, Van der Westhuizen, & Gieras, 2005). According to Wang *et al.,* their study has shown that about 18% of the losses is attributed to the Eddy current losses in axial-flux machine (Wang & Kamper, 2004b). Some papers have shown that only very little cogging torque exists within the air gap of an ironless stator (T. Chan & Lai, 2007; HÜNER & AKÜNER, 2012). According to (Hwang, Li, Chuang, Liu, & Huang, 2009), coreless AFPM machine design could eliminate cogging torque completely. Nevertheless, parasitic torque ripples still exist due to limitation in machine design. In this research, basic results of the Eddy current losses and cogging torque between the iron-core stator and coreless stator are compared. Therefore, detailed work dealing with cogging torque reduction and Eddy current elimination will be studied in the future.

Over the years, various optimization techniques and theories developed by engineers and scientists to enhance the electric machine structure with the aim to achieve desired characteristics within limitation. Huang *et al.* sizing equation was first derived to compute the power density equation for radial-flux permanent magnet (RFPM) machines, effective methods to compare the topologies of various electric machines were presented too. Other papers also derived the sizing equation for AFPM electric machines but no study on electric machine optimization was developed (Surong Huang et al., 1998). AFPM machines can be optimized with dimensional adjustment via geometrical parameters, output characteristic, analytical methods or soft computing methods. For instance, investigation on axial-flux permanent magnet coreless generator was done by Virtic *et al*. using magnetic equivalent circuit, and the proposed method is lack of dimensional modification (Virtič & Avsec, 2011). Chung *et al*. presented 3D electromagnetic finite element analysis and basic structure adjustment, but only 4 parameters (output power density, machine`s efficiency, maximum current density and maximum rms phase voltage) were considered as optimization parameters, The "Conjugate Gradient" was used as the optimization method which is found to be

unsuitable to solve a non-linear multi-objective function (Chung & You, 2014). Mirzaeian *et al*. presented a multi-objective optimization model utilizes the "Genetic-Fuzzy Algorithm (GFA)" for optimal design of a "Switched Reluctance Motor (SRM)" with high efficiency and low torque ripple as objective functions (Mirzaeian, Moallem, Tahani, & Lucas, 2002). In (Amin Mahmoudi, Kahourzade, Rahim, Ping, & Uddin, 2013), the authors introduce soft computing based on Genetic Algorithm method to optimize multi-objective slotted TORUS AFPM machine parameters, this method shows the tradeoffs between machine output power density and size. It is a method that minimizes the TORUS AFPM machine using various parameter considerations that include multiple dimensional variables in a non-linear fitness functions. In the aforementioned research subject, the design procedure was not considered using hybridization of two different optimization algorithms for multi-objective function search. Moreover, problems exist in the Genetic Algorithm such as slow convergence rate and easily fall into the partial optimum (Marinakis et al., 2010). As a result, the design parameter obtained by utilizing Genetic Algorithm may not be that accurate.

In this thesis, analytical and impact study of the hybrid optimization method into an AFPM coreless generator (AFPMG) is presented, the hybrid model improves the search function duration by reducing overall convergence rate and increases accuracy of the machine power density output. The thesis also highlights the novel hybrid optimization is used, the design of such generator, and the reason of such options are selected to achieve the desired objectives through simulation and experiment.

2.2 Types of Axial-Flux Permanent Magnet Machine

2.2.1 Single-Rotor Single-Stator Structure

Figure 2.1(a) shows the single-sided axial-flux permanent magnet machine (Campbell, 1974). This is the simplest AFPM configuration. However, unbalance axial

forces between the stator and rotor exist in this structure. As a result, a differential shaft bearing and a stiff rotor disc is recommended (C. C. Chan, 1987; Platt, 1989; Profumo, Zhang, & Tenconi, 1997). The magnetic force between iron stator and rotating permanent magnets may bend the structure, hence causes rotor fracture. With coreless stator, the axial force is minimum because it exerts on the copper windings, rather than on iron stator.

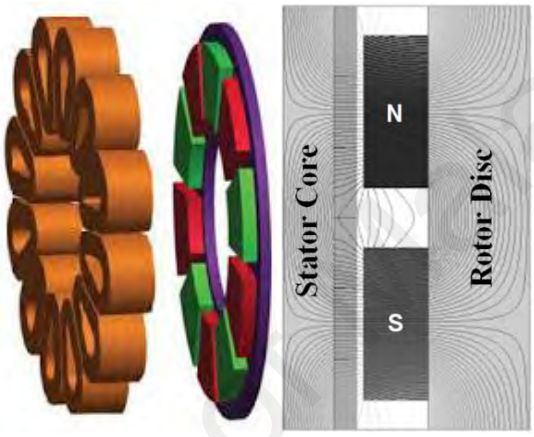

(a) (b)

Figure 2.1: (a) Single-sided AFPM machine. (b) Cross-section of AFPM magnetic flux path.

Figure 2.1(b) shows the flux paths in the ferromagnetic stator core and rotor yoke, it shows the side view of a surface-mounted permanent magnet and it is common magnet arrangement for the single-sided AFPM machine. The arrangement of permanent magnets and winding configurations can affect the machine`s flux path, hence altering the magnetic reluctant in rotor as well as stator.

2.2.2 Double-Rotor Single-Stator Structure

Figure 2.2(a) shows a single-stator double-rotor axial-flux permanent magnet machine that has its` phase windings wound around bobbins/stators or slotted-stators (S.

Gholamian, Ardebil, Abbaszadeh, & Charati, 2005). The stator windings are placed in air gap between two adjacent rotor discs. The magnetic field produced by permanent magnets on each rotor disc induces back-EMF in the windings while they rotate. Technically, a coreless stator and slotted-stator differ in terms of winding type and output characteristics. In a coreless structure, losses in permanent magnets and solid steel rotor discs are usually negligible, this type of design offers higher efficiency at zero cogging torque. A much larger volume of permanent magnets in comparison with laminated stator core AFPM machine is required in order to maintain a reasonable level of flux density in the air gap. In a slotless-stator structure, the end-windings are short, copper losses are less hence is expected to have better heat-dissipation of conductor. When operating at relatively high frequency, significant Eddy current losses in the stator winding conductors may occur, special coil wire/conductor may be necessary for some occasion. In industrial standard, epoxy resin are filled in between the air-gap portion and windings in order to increase the core robustness (Söderlund, Eriksson, Salonen, Vihriälä, & Perälä, 1996). Due to higher efficiency, this type of machine are used in propulsion machines and high speed generators (Eastham et al., 2002).

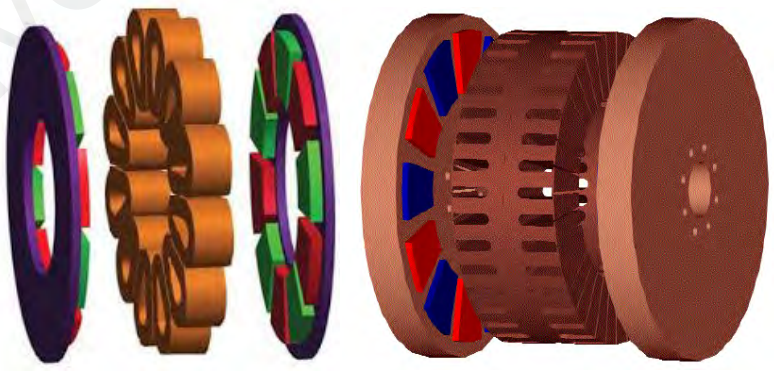

(a) (b)

Figure 2.2: (a) Double-sided AFPM machine. (b) "TORUS" type AFPM machine.

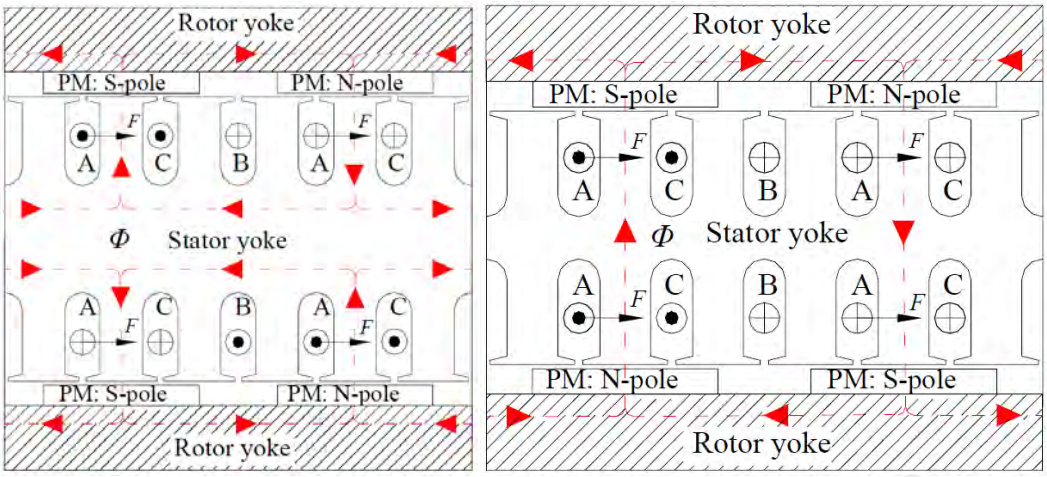

Figure 2.3: (a) North-North magnet arrangement. (b) North-South magnet arrangement.

Figure 2.2(b) is another variation of AFPM machine, it is called the "TORUS" type axial-flux permanent magnet machine, this type of machine has slots in its` stator yoke to allow coil winding (Muljadi, Butterfield, & Wan, 1999b; Spooner & Chalmers, 1992). Figure 2.3(a) and figure 2.3(b) show the North-North and North-South magnet arrangements, the phase-A coil tangential Lorentz forces are illustrated in both figures. The machine can be constructed by two single-sided AFPM machine as depicted in figure 2.1. For the North-North (NN) magnet structure, the end-windings in the machine are short in radial as well as in axial directions. A short end-winding reduces copper losses in stator coils while the flux flows around along the stator core. In order to increase flux confinement, a thicker stator yoke is used. As a consequence, this also increases the end-winding lengths and iron losses. In the North-South (NS) magnet structure, the main flux flows axially through stator, so a stator yoke is unnecessary. However, if to produce torque, lap windings are needed which in turn elogate the end-winding, As a result, longer end-winding again increases the copper losses (Locment, Semail, & Piriou, 2006; Takano, Itoh, Mori, Sakuta, & Hirasa, 1992).

In conclusion, to compare NN and NS structure, the external diameter of NN is smaller with less copper losses but expected to have more iron losses and is longer in

axial direction. For torque production, lap winding is used in NS structure while NN structure uses either end-winding or lap-winding. In AFPM coreless machine, the flux flows freely from one rotor side to another without being confined along any stator core. Thus, higher efficiency is expected in this type of AFPM machine (Caricchi, Crescimbini, Honorati, Di Napoli, & Santini, 1996; Lombard & Kamper, 1999).

2.2.3 Single-Rotor Double-Stator Structure

Alternative to single-stator double-rotor structure, figure 2.4 shows the permanent magnets located on both surfaces of a rotor disc sandwiched between two stator yokes. This single-rotor double-stator AFPM machine is also known as the axial-flux interior-rotor (AFIR) machine, it could be constructed in slotted or slotless/coreless configuration, the main flux flows circumferentially along the rotor disc and axially through the rotor disc. Figure 2.4(b) shows the "TORUS" stator structure that is slotted to wind in the phase coils (Parviainen et al., 2004; Platt, 1989; Qu & Lipo, 2003).

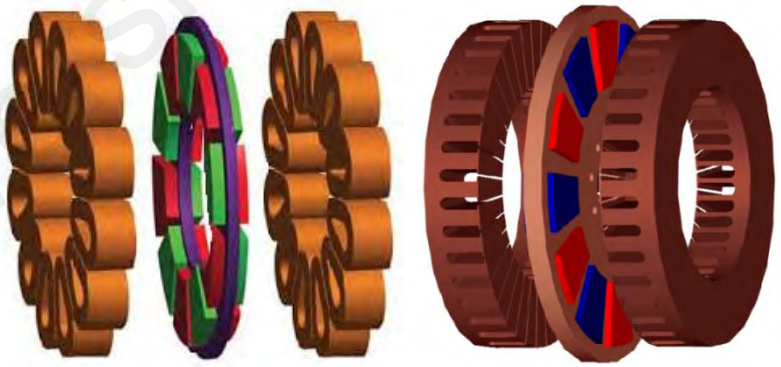

(a) (b)

Figure 2.4: (a) Double-stator single-rotor AFPM machine. (b) Single-rotor double-stators "TORUS " structure.

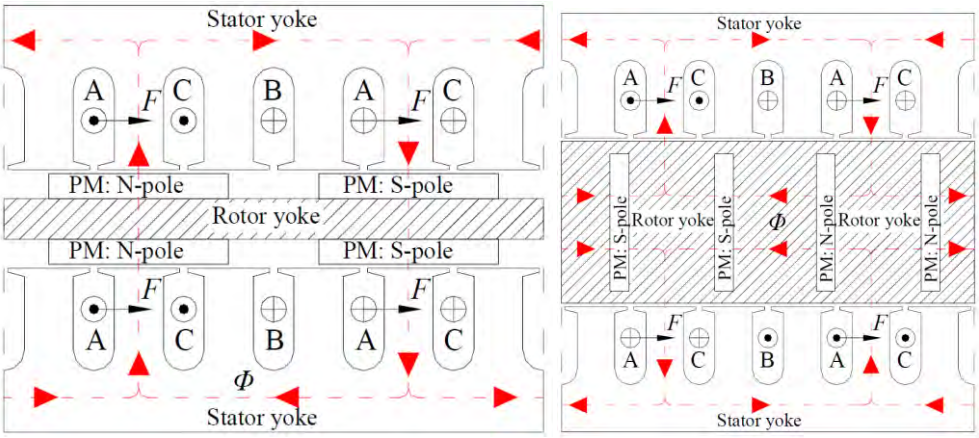

(a) (b)

Figure 2.5: (a) Surface-mounted permanent magnet rotor disc. (b) Embedded permanent magnet in a rotor core (buried PM).

Figure 2.5 shows the flux path in cross-sectional of two types of AFIR machine, it is also known as the AFIPM (Axial-Flux Interior Rotor Permanent Magnet) machine. The surface-mounted rotor structure in figure 2.5(a) uses thin rotor disc that requires strong materials such as Aluminum T6063. For the sake of maintaining similar machine structure, another alternative is to use thicker rotor disc with buried permanent magnets in it as shown in figure 2.5(b). Consequently, it is found that the power density is significantly reduced. In a surface-mounted structure, leakage flux in permanent magnet ends is higher in non-ferromagnetic material rotor (Metin Aydin, Huang, & Lipo, 2006). Moreover, the rotor thickness and inconsistent magnetization of permanent magnets along the machine radius may cause difficulties, depending on the machine diameter, number of poles and inner radius of the permanent magnets (Marignetti, Colli, & Carbone, 2010). At the machine outer radius, the flux density distribution is also found to be inconsistent in the air-gap along the machine radius. To compare both the surface-mounted structure and buried structure, it is found that the buried structure has higher armature reaction than the surface-mounted structure. The buried structure has better

permanent magnet protection against mechanical impacts such as oxidation and degradation.

2.2.4 Multi-Rotor Multi-Stator Structure

Multi-stage AFPM machines are rarely explained in most literatures review. A multi-stage AFPM machine is a cascade of several individual "Single-stator Single-rotor" and "Single-rotor Double-stator" structures lined up about the same shaft. In the event of limited radial diameter, multi-stage arrangement can boost the machine desired electromagnetic torque. This kind of machine structure gains its appropriative applications such as in aircraft propulsion (Eastham et al., 2002) and electric pump (Di Stefano & Marignetti, 2012). In addition, it is easier to assembly multi-stage AFPM machines compared to multi-stage radial-flux permanent magnet (RFPM) machines. Unlike RFPM machines, the air-gap distance can be maintained without changing the machine`s outer diameter. On the other hand, multi-stage RFPM machines are certainly much complex configuration and bulky. Figure 2.6 shows the AFPM machines with slotless-stator and slotted-stator structure.

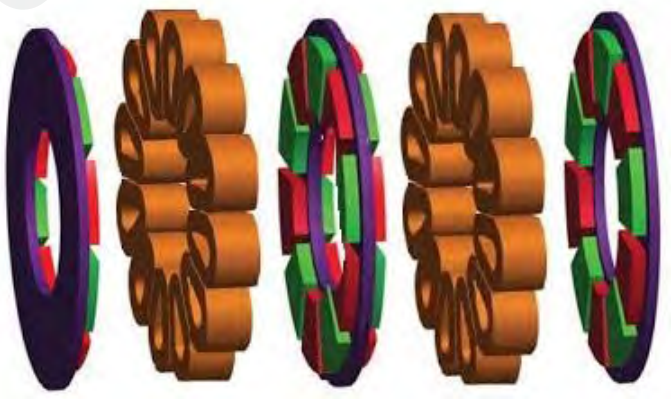

(a)

Figure 2.6: (a) Air-core multistage AFPM machine. (b) Multistage structure; triple-stator double-rotor.

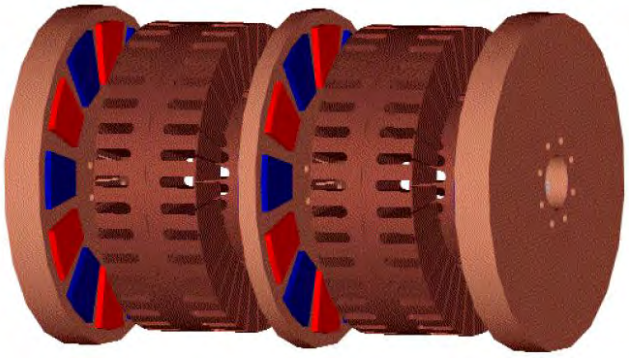

(b)

Figure 2.6, continued

Generally, a multi-stage AFPM machine has N number of stator with an additional N number of rotor disc. The stator and the rotor must be coupled to the same mechanical shaft in order to rotate about the same axis. Regardless of "TORUS" or coreless AFPM structure, an AFPM machine can be multiple multi-stage cascades. An AFPM machine with multi-stage configuration can be constructed with multiple rotor discs or with ironless armature windings, in which the magnetic field permeates along the machine in axial direction.

2.3 Analysis of Axial-Flux Permanent Magnet Machine

2.3.1 Electromagnetic Field Analysis

For accurately solve the electromagnetic field and performance problems related to integral equations and partial differential equations, several tools can be used such as the analytical, quasi-3D and Finite Element Method (FEM) (Azzouzi, Barakat, & Dakyo, 2005; Bumby et al., 2004; Kurronen & Pyrhönen, 2007; J. K. Lee, 1992; Marignetti, Colli, & Coia, 2008; Upadhyay & Rajagopal, 2006; Zhilichev, 1998). At present, FEM is a more accurate method compared to the other analytical methods. For the electromagnetic analysis in electric machine, the finite element analysis is a well-established design method. Despite the 2D and 3D FEM may have been a popular tool

for modeling, emphasis is also given on the optimization tool as well. Finite element analysis (FEA) is known to take long computation time, also with different geometry models require different mesh mapping to achieve better result. The prominent function of FEM is it can subdivide geometry into finite elements (tetrahedral elements) whereby a covering equation is applied. In each subdivided element, polynomial equation from the calculus is used to approximate a solution by minimizing an associated error function.

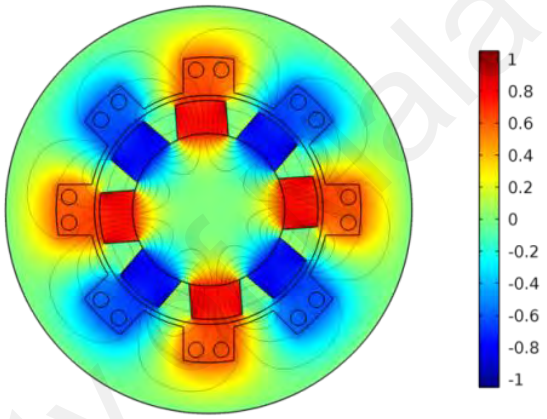

Figure 2.7: Flux density and symmetry conditions in a 2D FEA of a radial-flux PM machine.

Adequate meshing capability, robustness and adaptive solution technique are found in FEM. To apply this technique into electric machine analysis, the geometry is usually downsized to a quarter of the entire model in the interest to shorten the computation time using symmetry multiplier. Generally, a 2D plane FEA analysis is satisfactory for certain simple machine structure. However, in most complex machine structure, 3D FEA analysis is recommended to achieve more accurate result. The advantage of FEM comes with the ability to provide automated mesh, material database selection, boundary options, hence, FEA can be used to execute for solutions which require no prior knowledge of the numerical analysis. For example, figure 2.7 shows the

2D flux density color map and boundary conditions of a radial-flux permanent magnet machine.

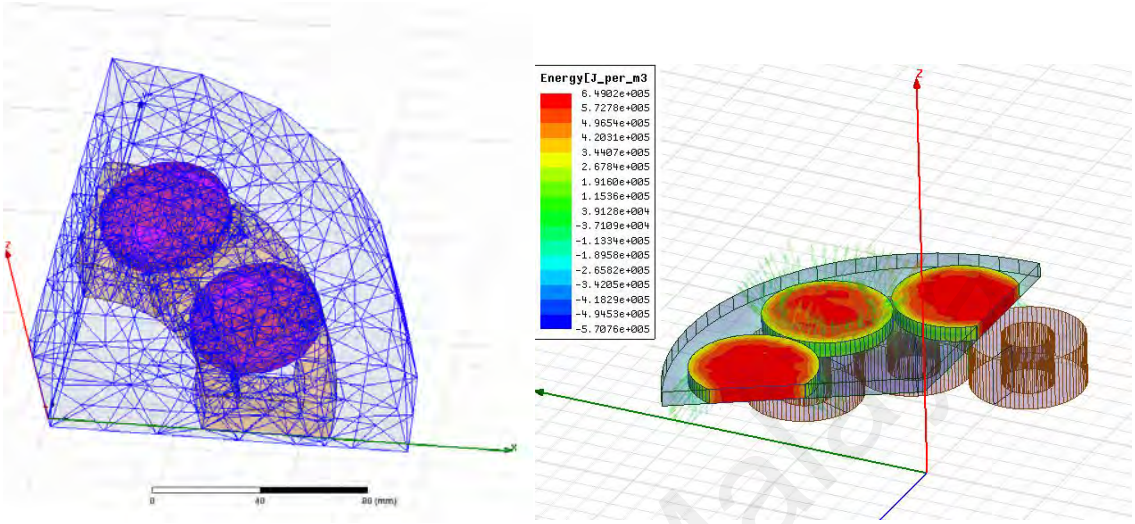

(a) (b)

Figure 2.8: (a) Geometry boundary with 3D meshing. (b) Flux-density plot of a reduced geometry.

The main consideration and analysis equations for FEM method are described in (Demenko, 1996; Nédélec, 1980). The description of the radial-flux permanent magnet machines and axial-flux permanent magnet machines are also shown in related paper (Upadhyay & Rajagopal, 2006). Contrary to the 2D FEA, the electromagnetic behavior appears in the 3D FEA of an electric machine can be plotted as shown in figure 2.8. The 3D FEA can also provide additional details about the end-winding inductance, torque and flux leakage lines. For a massive machine with very complex system can cause present-day computers insufficient to handle its` numerical analysis efficiently. However, this problem of long computation can be mitigated with the quasi-3D method. Figure 2.8(a) shows the smallest geometrical entity in 3D FEA, it can be seen that only one-fourth of the geometry is sufficient for modeling the structure of AFPM machine.

2.3.2 Torque Analysis

Minimization of cogging torque is often the objective in permanent magnet machine design. Torque is a conventional by-product of any permanent magnet machine, AFPM has no exception too. Torque ripples are produced in AFPM machine which affect the output performance. In iron-core AFPM machine, the main effects are the torque ripples, cogging torque and saturation of magnetic circuits. Theoretically, coreless-stator AFPM machine could be designed to get rid of cogging torque. Nevertheless, parasitic torque ripples do exist that contribute to the machine design limitation. In (M Aydin, Zhu, Lipo, & Howe, 2007; Jahns & Soong, 1996), several methods for minimizing torque ripples regarding AFPM machines are described, the techniques proposed include magnet shaping, magnet skewing, skewing of stator slots, slots adjustment and electronic drive control.

In this case study, a single-rotor double-stator AFPM machine is used as reference machine in 3D FEA (Parviainen et al., 2004; Qu & Lipo, 2003). The machine is solved in a magneto-transient setup to evaluate the torque ripple. Figure 2.9 displays the comparison of cogging torque between the 3D FEA and analytical method, the analytical model is shown to obtain higher peak cogging torque value. Also, it can be seen that both the graph curvatures are relatively similar. Another analytical method on cogging torque is also described in (Barakat, El-Meslouhi, & Dakyo, 2001; Kurronen & Pyrhönen, 2007), the authors show that it is possible to use analytical approach to evaluate the cogging torque up to certain degree of accuracy. Overall, the analytical method requires shorter time for computation compared to 3D FEA and is therefore preferred by some designers. Nevertheless, FEA is still a better option that involves detailed machine investigation because it can display detailed saturation points of different part of the AFPM machine.

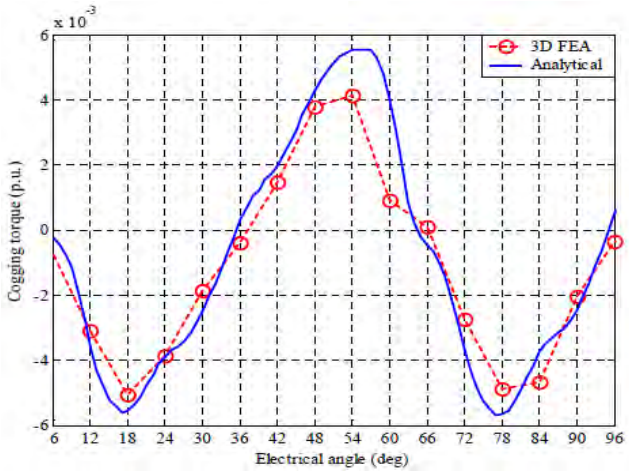

Figure 2.9: 3D FEA and analytical model comparison for cogging torque (Parviainen et al., 2004; Qu & Lipo, 2003).

2.4 Design Procedure of the AFPM Machines

The proposed AFPM generator has a single-rotor double-stator structure with two identical stator plates. The design does not incorporate any ferromagnetic material in its` core and is therefore does not incur any cogging torque and core losses. The basic structure of the AFPM coreless generator is shown in figure 2.4(a). The design procedure of the machine should achieve maximum output power density with desired sinusoidal back-EMF value that is maintained within the design restriction. To achieve this, optimization process adopted for the AFPM machine by altering its` geometrical parameters as well shape modification is done, in this case, certain geometrical parameters due to selected material or application characteristics may not be varied in the design procedure. Other optimization methods such as the Deterministic method uses numerical optimization procedure to optimize parameters, this method produces fast convergence in close-to-read value with the tendency to be trapped in local optimum. On the other hand, the Heuristic method and Probabilistic method are remarkably applicable to multi-objective optimization problems, with stringent requirement of good initial values estimation; this method is extremely time consuming which gives itself a big disadvantage. However, with new powerful computer

processing speed, new development of modern algorithm packed in efficient software has resulted in soft-computing method the best choice for optimizing AFPM machine.

Figure 4.2 shows the optimization flowchart for the AFPM coreless generator using hybrid optimization GA-PS method. Although there are multiple tools to perform hybridization, hybrid GA-PS model is chosen because it is easily accessible in the MathWorks development environment or programmable in other programming language. In the hybrid model, GA in MATLAB initializes the initial population based on preset generated population and all the candidates are to be vectorized in m x n matrix, usually in the form of multiple-column single-row matrix as shown in section "Crossover Operator". Then, the first fitness value based on minimized fitness function variables is calculated and the best fitness value (Elitist) is selected. Followed by crossover, genes from each parent are intervened and the similar number of new child/offspring generation is created. Finally, a small mutation probability ratio is imposed on randomly selected chromosomes. Upon reaching the set stopping criteria, the best value of variables with the best fitness function value is delivered to the next Pattern Search algorithm to perform search computation. In Pattern Search algorithm, all previously returned values are added to the mesh size in a pattern vector. The algorithm calculates the objective function at mesh points until it spots one which the value is smaller than the previous smallest value (Cao & Wu, 1999; Dao et al., 2016). In a large population, the hybrid GA-PS algorithm searches the solution space more thoroughly, thereby confirms the function converges to the global minimum (Amrita & Mohan Rao, 2011). However, this algorithm runs more slowly with a larger population size subject to its` preset generation. To implement this algorithm, a MATLAB GUI optimization tool was developed that follows the GA-PS optimization process as discussed above. Comparison among GA, PS and hybrid GA-PS are discussed in chapter 5.

2.5 Applications of AFPM Machine

Various applications require AFPM machine structure, they are most commonly used in wind generators and vehicle propulsions. The primary reason for such interest is due to better power electronic components. In addition, better construction materials were found over the last decades have contributed the advancement too (Parviainen et al., 2004; Qu & Lipo, 2003). In 1992, a 2.5kW AFPM engine-driven toroidal stator generator was developed (Spooner & Chalmers, 1992). Low-speed direct drive AFPM synchronous 100kW wind turbine generator was also designed by the same authors. According to Pullen *et al.*, gas turbine incorporated with high speed AFPM generator can be used in a hybrid traction system (Pullen, Etemad, & Fenocchi, 1996). Hybrid AFPM generator-motor in electric vehicle with flywheel was introduced in 1996 (Acarnley et al., 1996). In the same year, a slotless stator 880W AFPM adjustable-speed pump was developed by (Caricchi, Crescimbini, & Honorati, 1998). In ship propulsion technology, AFPM machine with slotless toroidal iron stator was described by (Caricchi, Crescimbini, & Santini, 1995), this technology uses two direct-driven counter rotating propellers for propulsion. In power generation applications, large air-gap diameter with high tangential force direct-drive wind turbines generator was described by Chan *et al.* (T. Chan & Lai, 2007). In 2002, Eastham *et al.* introduced a unique direct-drive brushless AFPM machine for aircraft technology (Eastham et al., 2002). In (Chen, Pillay, & Khan, 2005; Parviainen et al., 2004; Qu & Lipo, 2003), various surface-mounted permanent magnet AFPM machines are also presented. AFPM machines with air-core stator windings have recently gained its popularity, this is because there is no cogging torque in the machine and is regarded as highly efficient machine (Wang & Kamper, 2004a).

CHAPTER 3: THEORY OF AXIAL-FLUX PERMANENT MAGNET MACHINES

3.1 Introduction

In order to study the AFPM machine, it is necessary to use theoretical approach to understand parameters that affect the output of generator. This chapter presents the theories and derivations of the basic electrical machine and electromagnetic parameters. Hence, derivations of all design variables such as the winding factors, permanent magnet span, EMF waveform and number of winding configurations are shown.

3.2 Basic Equations

3.2.1 Torque

In torque analysis, a circular permanent magnet produces square wave flux density distribution, B_{max}. It is also assumed the wire is carrying a current $\vec{\imath}$ through a conductor length $\vec{l}$. The Lorentz force and torque equation of the AFPM machines can be derived as;

$$\vec{F} = \vec{l}.(\vec{\imath} \times \vec{B}) \tag{3.1}$$

A torque is produced when force is exerted at a radius ($\vec{r}$).

$$\vec{\tau} = \vec{r} \times \vec{F} \tag{3.2}$$

Figure 3.1 shows the direction of interacting magnet flux and stator in a basic AFPM machine. In order to derive torsion equation in equation (3.2), the sinusoidal ampere conductor distribution is to be formalized at first.

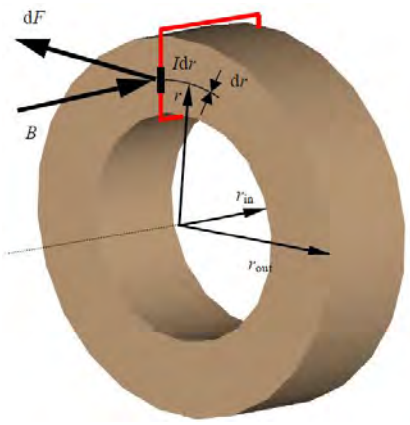

Figure 3.1: Torque production vector in an axial-flux machine.

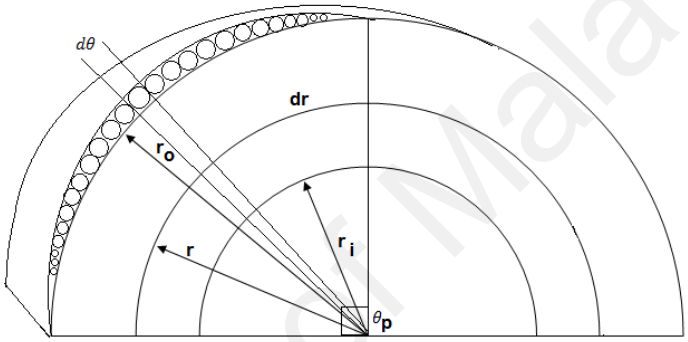

Figure 3.2: Sinusoidal distributed conductors of one phase on the stator pole section.

As seen in figure 3.2, inside the stator current sheet depicts the sinusoidal flux density distribution in the air gap. The number of conductors wire per phase at any incremental angle $d\theta$, the number of conductors considering only one phase is;

$$\frac{N_{s-ph}}{2}\sin(p\theta)d\theta \tag{3.3}$$

Where $d\theta$ is the incremental angle, p is the number of pole pairs and N_{s-ph} is the sinusoidal distributed series turns per phase. Since there are $2N_p$ conductors in one pole, the integration of equation (3.3) over a pole pitch gives the total number of conductor turn per pole as shown in equation (3.4). Now to consider three phase windings, whose axes are 120 electrical degrees apart with a perfect sinusoidal current waveform. The total amount of current flowing through an incremental angle $d\theta$ at the

time *t* can be derived by adding up the contributions of all three phases (Niazi, Toliyat, Cheong, & Kim, 2007), the phase current are shown in equation (3.5);

$$2N_p = \frac{N_{s-ph}}{p} \tag{3.4}$$

$$\begin{bmatrix} Phase\ A: i\cos(\omega t)\frac{N_s}{2}\sin(p\theta)d\theta \\ Phase\ B: i\cos\left(\omega t - \frac{2\pi}{3}\right)\frac{N_s}{2}\sin\left(p\theta - \frac{2\pi}{3}\right)d\theta \\ Phase\ C: i\cos\left(\omega t + \frac{2\pi}{3}\right)\frac{N_s}{2}\sin\left(p\theta + \frac{2\pi}{3}\right)d\theta \end{bmatrix} \tag{3.5}$$

Finally, the yield is derived as following;

$$\frac{3}{2}I\sqrt{2}\frac{\mathrm{N_s}}{2}\sin(p\theta - \omega t)d\theta \tag{3.6}$$

Where *I* is the RMS current value and *i* is the amplitude of the phase currents. The air-gap flux density due to the permanent magnets is;

$$B_{g1}(\theta) = B_{g1}cos(p\theta - \omega t - \alpha) \tag{3.7}$$

Where the amplitude of the fundamental component is B_{g1}, the electrical angle between stator and rotor is α. Until equation (3.7), the magnet flux density and ampere-conductor distribution had been derived. Now, it is to determine the torque of the AFPM machine using equation (3.1) and equation (3.2). By integrating the incremental torque at radius *r* from r_i to r_o as seen in figure 3.2, the "incremental force" over area span of $d\theta \times dr$ is derived as;

$$dF_l(r,\theta) = B_{g1}cos(p\theta - \alpha)\frac{3}{2}I\sqrt{2}\frac{N_s}{2}\sin(p\theta)\,d\theta dr \tag{3.8}$$

After eliminating the time dependent term ωt in equation (3.6), the total force at radius *r* for one pole can be found by integrating equation (3.8) from angle 0 to π/p (i.e.

the angular pole pitch) and for the whole stator unit the equation must be multiplied by the number of poles (2 p);

$$F_l(r) = 2p \int_0^{\frac{\pi}{p}} B_{g1} cos(p\theta - \alpha) \frac{3}{2} I\sqrt{2} \frac{N_s}{2} \sin(p\theta)\, d\theta dr \tag{3.9}$$

Finally, using equation (3.2);

$$\tau_l(r) = 2p \int_0^{\frac{\pi}{p}} B_{g1} cos(p\theta - \alpha) \frac{3}{2} I\sqrt{2} \frac{N_s}{2} \sin(p\theta)\, d\theta dr \tag{3.10}$$

And the fundamental torque for one stator face of the AFPM machine is found by solving the integral equation as;

$$\tau_l(r) = 2p \int_{\tau_i}^{\tau_0} \int_0^{\frac{\pi}{p}} B_{g1} cos(p\theta - \alpha) \frac{3}{2} I\sqrt{2} \frac{N_s}{2} \sin(p\theta)\, d\theta dr \tag{3.11}$$

$$\tau_l = \frac{3}{8}\sqrt{2}\pi B_{g1} N_s I\, (\mathrm{r_0}^2 - \mathrm{r_i}^2)\sin(\beta) \tag{3.12}$$

Where $\beta = -\alpha$, which is known as the torque angle of a synchronous machine. Practically, it is quite impossible to place the conductors sinusoidally. For a more realistic and practical equation, the actual number of series turns per phase N_{ph} is included in the equation by defining the effective number of sinusoidally distributed series turns per phase N_s (Jiang & Jahns, 2015);

$$\mathrm{N_s} = \frac{4}{\pi} k_{w1} N_{ph} \tag{3.13}$$

Where k_{w1} is the fundamental winding factor which contains the effects of distributed, shortened and skewed windings. The torque formula reduces to;

$$\tau_l = \frac{3}{2}\sqrt{2} B_{g1} k_{w1} N_{ph} I(r_o{}^2 + r_i{}^2) \sin(\beta) \tag{3.14}$$

The torque equation can also be represented in terms of the effective length of stator and average diameter and as;

$$\tau_l = \frac{3}{2}\sqrt{2}B_{g1}k_{w1}N_{ph}ID_{ave}\sin(\beta) \tag{3.15}$$

Where $D_{ave} = r_o + r_i$. In order to simplify the design calculations, a parameter "stator-surface current density" or "specific electric loading" as it is called in the literature, should be inserted in the equations, because typical values of the surface current density for different applications are practically known, which helps for identifying initial design parameters. The amplitude of the surface current density (K_l) ranges from 10000 A/m for small motor to 40000 A/m for medium power motors (C. Chan et al., 1996). This parameter shows how many amperes can be packed together in each unit length of the stator circumference. The value is limited of course by several factors such as cooling, slot depth and slot fill factor (Niazi et al., 2007). Since there are 3 phases, $2N_{ph}$ conductors in each phase and $\sqrt{2}I$ as the peak current, the fundamental component of the surface current density K_l is defined as;

$$\mathrm{K}_l = \frac{total\ max.ampere - conductors}{armature\ cirumference} = \frac{3\sqrt{2}I2N_{ph}}{D_{ave}\pi} \tag{3.16}$$

Due to the particular structure of the AFPM machines, the average diameter of the stator is used for calculation of the armature circumference. By eliminating $N_{ph}I$ in equation (3.15) using equation (3.16), the torque equation becomes;

$$\tau_l = \frac{1}{4}\pi B_{g1}k_{w1}K_l D^2{}_{ave}\,L_i\sin(\beta) \tag{3.17}$$

Where $L_i = r_o - r_i$. Since this torque equation is calculated only for one stator face, it can be generalized by multiplying the expression with parameter *h* to obtain the total torque of an AFPM machine with *h* stator faces as;

$$\tau_l = \frac{h}{4}\pi B_{g1} k_{w1} K_l D^2{}_{ave} L_i \sin(\beta) \tag{3.18}$$

The torque can also be written in terms of outside radius of the stator r_0, the factor λ (r_i/r_0), which is the ratio of inside to outside radius of the stator, is inserted in the equation as;

$$\tau_l = \frac{h}{4}\pi B_{g1} k_{w1} K_l r_0{}^3 (1-\lambda^2)(1+\lambda) \sin(\beta) \tag{3.19}$$

As derived in equation (3.19), it is clearly shown that the outside radius of the stator and the factor λ affect the machine torque generation. This is the most important sizing equation of AFPM machines.

3.2.2 Back-EMF and Power

According to Faraday`s Law of Induction, a voltage *e* is induced in a conductor with length *l* moving with a velocity $\vec{v}$ cutting the flux line in amagnetic field $\vec{B}$, the voltage *e* is written as;

$$e = \oint (\vec{v} \times \vec{B}) \, . \, dl \tag{3.20}$$

As seen in figure 3.1, the rotor rotates with velocity $\vec{v}$ which is perpendicular to the direction of magnetic field. To calculate back-EMF of each phase by referring figure 3.2, it utilizes the fundamental components of air-gap flux density in equation (3.7). Assuming the conductor length equals $L_i = r_o - r_i$, the induced back-EMF in the conductors can be written as;

$$de = B_{g1}(\theta) L_i v \frac{N_s}{2} \sin(p\theta) \, d\theta \tag{3.21}$$

If the mechanical speed of the rotor is ω_m, the average circumferential speed of the conductor is;

$$v = \omega_m \frac{D_{ave}}{2} \tag{3.22}$$

Substitute equation (3.22) in equation (3.21) results;

$$de = B_{g1}(\theta) L_i \omega_m \frac{D_{ave}}{2} \frac{N_s}{2} \sin(p\theta)\, d\theta \tag{3.23}$$

Using equation (3.7);

$$de = B_{g1} \cos(p\theta - \omega t - \alpha)\, L_i \omega_m \frac{D_{ave}}{2} \frac{N_s}{2} \sin(p\theta)\, d\theta \tag{3.24}$$

Which results in;

$$de = B_{g1} \omega_m \frac{D_{ave}}{2} L_i \frac{N_s}{2} \frac{1}{2} [\sin(p\theta - \omega t - \alpha) + \sin(\omega t + \alpha)]\, d\theta \tag{3.25}$$

Integrating equation (3.25), the fundamental component of the instantaneous phase back-EMF for a machine with p pole pairs can be calculated;

$$e_l = 2p \int_0^{\frac{\pi}{p}} de = 2p \int_0^{\frac{\pi}{p}} B_{g1}\, \omega_m \frac{D_{ave}}{2} L_i \frac{N_s}{2} \frac{1}{2} [\sin(2p\theta - \omega t - \alpha) + \sin(\omega t + \alpha)]\, d\theta \tag{3.26}$$

After integral, the idealized back-EMF is as below;

$$e_l = \frac{\pi}{2} \int_0^{\frac{\pi}{p}} B_{g1}\, \omega_m \frac{D_{ave}}{2} L_i N_s \sin(\omega t + \alpha) \tag{3.27}$$

This equation is only assumed to have idealized sine wave output and it only represents the fundamental components. Substitute equation (3.13) into equation (3.27), the RMS phase back-EMF equation can be written as;

$$E_{ph} = \frac{\sqrt{2}}{2} B_{g1} \omega_m k_{w1} N_{ph} D_{ave} L_i \tag{3.28}$$

Finally, the apparent electromagnetic power of the three phase machine can be calculated by cross product of equation (3.16) and equation (3.28);

$$S_{elm} = 3hE_{ph}I = \pi \frac{h}{4} B_{g1} \omega_m k_{w1} K_l D^2{}_{ave} L_i \tag{3.29}$$

3.2.3 Rotating Permanent Magnets

Magnetic flux is created by the presence of permanent magnets, it influences the torque in the rotating machine. Therefore, the rotor design is a very important factor. There are two permanent magnet mounting methods; surface-mounted and interior mounted. Here, a simplified calculation of the required lengths of the permanent magnets for both structures is shown.

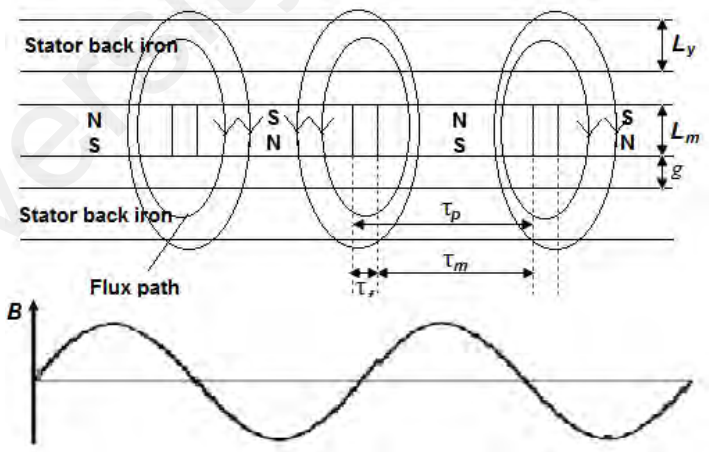

Figure 3.3: Air-gap flux density in a cross-section of the surface-mounted AFPM machine.

According to the axial cross-sectional picture shown in figure 3.3, the air-gap flux density equation can be derived as;

$$\nabla \times \vec{H} = \vec{J} \tag{3.30}$$

By neglecting the permanent magnet leakage flux and infinite permeability stator iron. The magnetic circuit approximation is written as;

$$2H_m L_m + 4H_g g = 0 \tag{3.31}$$

$$H_m = \frac{-2B_{g0} g}{\mu_0 L_m} \tag{3.32}$$

$$B_m = \mu_0 \mu_r H_m + B_r \tag{3.33}$$

Where B_m, H_m, B_{g0} and H_g are the permanent magnet, air-gap flux densities and field strengths respectively. B_r and μ_r are the permanent magnet remanence and relative permeability. Here the term B_{g0} corresponds to the average air-gap flux density as seen in figure 3.3. Putting equation (3.32) into equation (3.33) while assuming there is no tangential flux density component ($B_{g0} = B_m$), the air-gap flux density can written as;

$$B_{g0} = \frac{B_r}{1 + \frac{2g\mu_r}{L_m}} \tag{3.34}$$

Equations (3.34) is only derived for simplest design, however this method can be further refined by the inclusion of magnet leakage factor and slot coefficients (C. Chan et al., 1996). Besides, if there are no slots in the stator core, this increases the air-gap length effectively such the winding width is also covered as well.

To obtain good distribution of flux density on the surface-mounted permanent magnets, the magnet thickness can be shaped at the pole edges or a shorter permanent magnet pole arc can be used. In figure 3.4, the flux density distribution of a rectangular

permanent magnet, armature reaction and the resultant flux density waveforms are shown.

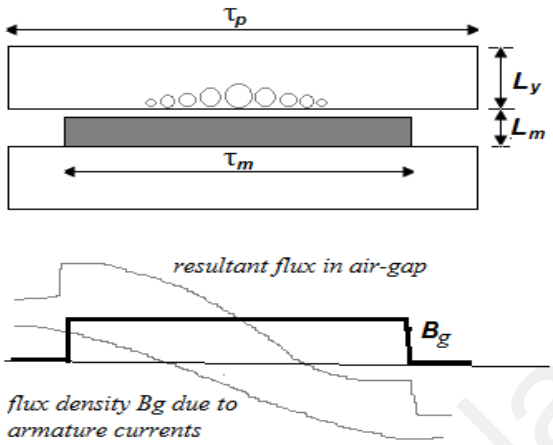

Figure 3.4: Flux density distribution of a sinusoidal current sheet and a rectangular magnet.

In figure 3.4, θ_m is the magnet span in electrical degrees. As an illustrative example, the amplitude of the first harmonic component is calculated from the Fourier analysis below. Since the air-gap flux density distribution is symmetric with respect to the orthogonal axis, the sine terms (in the function) are zero. Hence, the amplitude of the first harmonic component results in;

$$B_{g1} = \frac{1}{\pi}\left(\int_{-\frac{\theta_m}{2}}^{\frac{\theta_m}{2}} B_{g0}\cos\theta d\theta + \int_{\pi-\frac{\theta_m}{2}}^{\pi+\frac{\theta_m}{2}} B_{g0}\cos\theta d\theta \right) \tag{3.35}$$

$$B_{g1} = \frac{4}{\pi} B_{g0}\sin(\frac{\theta_m}{2}) \tag{3.36}$$

In this thesis the detailed electromagnetic analysis is left to the finite element analysis.

3.3 Design Variations

3.3.1 Permanent-Magnet Span

Optimum permanent magnet spans are different for various number of stator slots and winding configurations. Figure 3.4 shows the approximate flux density waveform with the surface-mounted permanent magnets. Since the flux density distribution is a symmetric function, the sine-terms in the Fourier expansion reduced to zero. The magnet flux density waveform can be represented in terms of a Fourier Series as shown;

$$B_m(\theta) = \sum_{n=1}^{\infty} B_n \cos(n\theta) \tag{3.37}$$

Where the general form for each harmonic component can be written as;

$$B_m(\theta) = \frac{B_{g0}}{n\pi}\left\{\sin\left(n\frac{\theta_m}{2}\right) - \sin n\left(\pi + \frac{\theta_m}{2}\right) + \sin n\left(\pi - \frac{\theta_m}{2}\right) - \sin n\left(2\pi - \frac{\theta_m}{2}\right)\right\} \tag{3.38}$$

It is obvious from the previous equation that the magnitude of the flux density harmonic components is directly dependent on the permanent magnet span. The minimization of these higher order harmonic components is essential considering the fact that all the flux components are rotating asynchronously with respect to the rotor and therefore cause losses in the stator.

3.3.2 Winding Factors

Winding factors take into account the reduction of the fundamental and other harmonic components due to the actual distribution of the windings (Niazi et al., 2007)

$$E_n = \frac{\sqrt{2}}{2} B_{gn}\, \omega_m\, k_{wn}\, N_{ph}\, D_{ave}\, L_i \tag{3.39}$$

Where E_n is the RMS value of the n[th] order EMF harmonic component. For instance, the coils can be deliberately under pitched or over-pitched to reduce certain harmonics, or the coils of the windings or permanent magnets can be facilitated to reduce the cogging torque (Niazi et al., 2007) in a conductive stator core. The winding factor k_{wn} has three components;

$$k_{wn} = k_{dn} k_{sn} k_{pn} \tag{3.40}$$

Where is k_{dn} is the distribution factor, k_{sn} is the skew factor and k_{pn} is the pitch factor. It can be seen that the distribution of coils of a phase can be easily achieved technically. The distribution factor or the spread factor is derived as (Niazi et al., 2007);

$$k_{dn} = \frac{\sin(n\frac{n_{spp}\,\theta_s}{2})}{n_{spp}\,\sin(n\frac{\theta_s}{2})} \tag{3.41}$$

Where n is the number of harmonic component, θ_s is the slot pitch in electrical degrees if it is an integral slot winding and n_{spp} is the number of stator slots per pole per phase. The windings of the coils can be made under or over-pitched to eliminate some of the higher harmonic components, but the fundamental component also being reduced. The reduction is represented by the pitch factor;

$$k_{pn} = \frac{n^{th}\ mean\ flux\ for\ the\ pitched\ coil}{n^{th}\ mean\ flux\ for\ full-\ pitched\ coil} = \sin(n\frac{\theta_c}{2}) \tag{3.42}$$

Where θ_c is the coil pitch in electrical degrees where the full pitch equals 180[o]. Skewing of the windings or the permanent magnets can be necessary to reduce the cogging torque, where the reduction of the induced voltage can be represented by the skew factor;

$$k_{sn} = \frac{n^{th}\ mean\ flux\ for\ the\ skewed\ design}{n^{th}\ mean\ flux\ for\ the\ unskewed\ design} = \frac{\sin(n\frac{\gamma}{2})}{n\frac{\gamma}{2}} \tag{3.43}$$

Where γ is the electrical angle of the skew. For AFPM machines however, the effect of changing the tooth width within the diameter of the disc should be taken into account when the permanent magnets are skewed.

3.3.3 Number of Stator Slots

Selecting the number of stator slots is important in order to reduce the cogging torque and harmonics components (Schwarz, 1991). For an 8-pole, three-phase AFPM machine, the winding configuration used is the concentrated coil winding. The multiple of three for the phase symmetry are 3, 6, 9, 12, 15 and 18. Due to winding structure and the diameter ratio, 12 winding slots is chosen as to simplify the prototype construction. Table 3.1 tabulates the number of slots per pole per phase n_{spp} with respect to machine slot number n_s.

Table 3.1: Slot numbers and the corresponding number of slots per pole per phase

Number of slot (n_s)	**Number of stator slots per-pole per-phase (n_{spp})**
3	0.25
6	0.5
9	0.75
12	1
15	1.25
18	1.5

Table 3.1 shows that fractional number found in the number of stator per pole per-phase are 3, 6, 9, 15 and 18. It is uncommon practice to use fractional-slot stator probably some of them have never been constructed. It should be noted that the winding arrangement of the fractional slot stators are not as straight forward as in the case of

integral-slot stators, and there can be more than one way for the designer to place the coils optimally (Niazi et al., 2007).

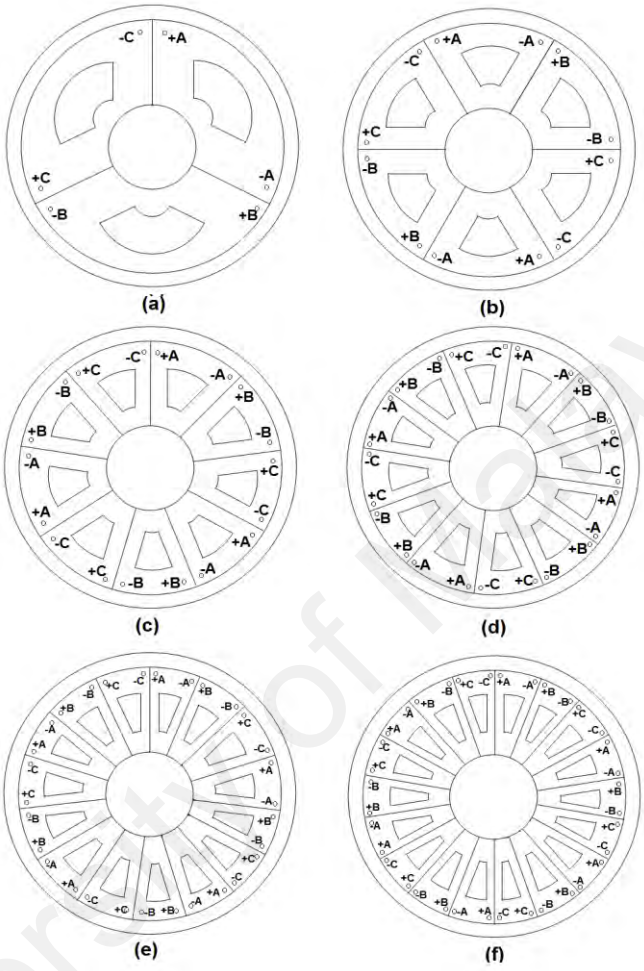

Figure 3.5: Stator winding configurations for 3, 6, 9, 12, 15, 18 stator slots.

3.3.4 Winding Configurations

Types of winding configuration are infinite. According to Rahman *et al.*, a distinct consideration method is applied to determine the coils placement (Rahman & Zhou, 1996), the method considers the following assumptions for the winding design;

a) An electric machine with three-phase.

b) The number of slot is multiple of the number of phases with all slots if filled.

c) All coils have similar coil turns and span equal slots number.

d) All similar size coils have same resistance and inductance.

e) Symmetrical coil arrangement where the back-EMF of phase A and phase B is 120 degree difference.

Table 3.2 shows the possible winding configuration as per use of coil arrangements in figure 3.5, there are coil arrangement for 9, 12, 15, 18, 21 and 24 stator slots. The pitching of the winding configuration can be altered by fractional-slot. Through FEA, all possible permanent magnet spans, winding configuration, induced back-EMF, losses and torque components were examined. By comparison of copper losses, the best is full-pitched 12-slot while 24-slot full-pitched the worst.

Table 3.2: Various configuration of winding pitch and the number of slots in each pole pair per phase

Number of stator slot	**No of poles**	**Coil pitch/ Pole pitch**	**Number of stator slots in each pole pair per phase (n_{spp})**
9	8	0.889	0.75
12	8	0.667	1
12	12	Fully pitched	1
15	8	0.533	1.25
15	12	0.8	1.25
18	12	0.667	1.5
18	16	0.889	1.5
21	12	0.571	1.75
21	16	0.762	1.75
21	20	0.952	1.75
24	16	0.667	2
24	20	0.833	2
24	24	Fully pitched	2

CHAPTER 4: DESIGN OPTIMIZATION, METHODOLOGY AND ANALYSIS

4.1 Introduction

Random search method, Hooke-Jeeves method, Powell method, and Genetic Algorithm are popular optimization techniques (Coello Coello & Christiansen, 1999; K. S. Lee & Geem, 2005)**.** The Powell method can achieve a solution fast but is not able to solve complex problem such as the Van Valedhuizen's wave function. On the other hand, the Hooke-Jeeves method is more accurate but is slower (Kahourzade, Mahmoudi, Ping, & Uddin, 2014). "Conjugate Gradient" is another method that is implemented as an iterative algorithm applicable to sparse systems that are too large to be handled by direct implementation, which is not suitable to solve a non-linear multi-objective function (Chung & You, 2014). "Genetic-Fuzzy Algorithm (GFA)" is a method that uses fuzzy systems constructed by using Genetic Algorithm, this method has slow convergence speed and easily fall into the partial optimum (Marinakis et al., 2010). However, there are also reported methods that are able to accelerate the optimization process and enhance the fitness function accuracy.

Designing an AFPM generator is basically a multi-dimensional optimization problem with several constraints. Since the optimization problem is a non-linear and several design parameters vary simultaneously, a hybrid optimization method is proposed to investigate the generator of its` kind. The prototype generator is optimized using the hybrid Genetic Algorithm-Pattern Search based on sizing equation function, and that generator will be used as reference design throughout this chapter. The prototype AFPM generator is analyzed using the finite element analysis, the thesis highlights the hybrid optimization used, the design of such generator, and the reason of such options are selected to achieve the desired objectives through simulation and experiment works.

4.2 Design Procedure

In order to maximize the efficiency while maintaining satisfactory output characteristics with respect to several constraints, such as permanent magnet demagnetization, leakages, losses and etc. The whole procedure requires dimensional evaluation, optimization, simulation and prototype construction and experiment which will be discussed in the following sections. The design procedure is summarized as follows;

i) Determine the application requirements

ii) Make structural decisions whether one-rotor or stacked configuration

iii) Determine the machine`s electric and magnetic loadings

- Phase current
- Terminal voltage
- Maximum allowable stator surface current density
- Air-gap flux density
- Maximum allowable flux density

iv) Determine the geometrical and physical constraints

- Air-gap length
- Stator outer diameter
- Stator inner to outer diameters ratio

v) Determine the dimensions of the stator and rotor

vi) Determine the permanent magnet type and stator type and dimensions

vii) Determine the losses

viii) Determine the efficiency

ix) Verify results with Finite Element Analysis

x) Verify results with experiment

4.3 Sizing Equations

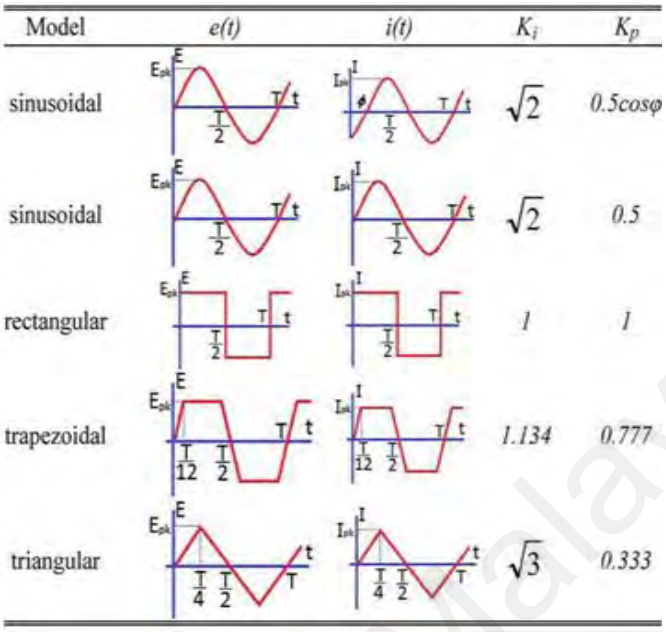

Figure 4.1: Typical prototype waveform factor.

A good electric machine design incorporates substantial good design knowledge and machine design theory. The sizing equation is one of the basic machine design knowledge acquired into this design. According to Huang *et al*. sizing equation derivatives, the sizing equation shows that the electric machine output power is interdependent on the design dimensions (Surong Huang et al., 1998). If stator leakage resistance and inductance are neglected, the general output power for any electric machine is calculated by using;

$$P_{out} = \eta \frac{m}{T} \int_0^T e(t) \cdot i(t) dt = m\eta K_p E_{pk} I_{pk} \tag{4.1}$$

Where *e(t)* and E_{pk} are air gap phase EMF and the peak value. The current *i(t)* and I_{pk} are the phase current and the peak phase current value, m is the number of machine phases, η is the machine efficiency and T is the period of one cycle of EMF (S. A. Gholamian, Ablouie, Mohseni, & Jafarabadi, 2009). K_p is the electrical power-

waveform factor and, K_i is the current waveform factor (S Huang et al., 1997; Ali Mahmoudi et al., 2013), the typical value for electrical power power-waveform factor, K_p is 0.5 and the current-waveform factor, K_i is $\sqrt{2}$ as shown in figure 4.1. The K_p is defined as;

$$K_p = \frac{1}{T}\int_0^T \frac{e(t)\cdot i(t)}{E_{pk}\,.\,I_{pk}}dt = \frac{1}{T}\int_0^T f_e(t)\cdot f_i(t)dt \tag{4.2}$$

$f_i(t)$ and $f_e(t)$ are the expressions for current waveform and normalized back-EMF. K_i for the current effect is defined as;

$$K_i = \frac{I_{pk}}{I_{rms}} = \frac{1}{\sqrt{\frac{1}{T}\int_0^T \left(\frac{i(t)}{I_{pk}}\right)^2 dt}} \tag{4.3}$$

Where I_{rms} is the phase-current root mean square (rms) value. The peak value of the phase air-gap back-EMF in equation (4.2) is expressed as;

$$E_{pk} = \frac{d\Lambda}{dt} = K_e N_{ph} B_g \frac{f}{P}(1-\lambda^2){D_o}^2 \tag{4.4}$$

Where f is the machine frequency, Λ is the air gap flux linkage per phase, K_e is the EMF factor, N_{ph} is the number of turns per phase, B_g is the flux density in air gap, P is the machine pole number in pair and the winding factor is K_w. The diameter ratio λ is equals to ${D_i}/{D_o}$. The diameter ratio is defined as;

$$\lambda = \frac{D_i}{D_o} \tag{4.5}$$

D_i is the inner surface diameter and D_o is the outer surface diameter. The peak phase current in equation (4.2) is expressed as;

$$I_{pk} = A\pi K_i \frac{(1+\lambda)}{2}\frac{D_0}{2m_1 N_{ph}} \tag{4.6}$$

Where $\boldsymbol{m_1}$ and A are the number of phases in each stator and electrical loading value. The derived sizing equation in term of $\boldsymbol{D_0{}^2 L_e}$ is presented as;

$$P_{out} = \frac{1}{1+K_{\emptyset}} \frac{m}{m_1} \frac{\pi}{2} K_e K_i K_p K_L \eta B_g A \frac{f}{P} (1-\lambda^2) \left(\frac{1+\lambda}{2}\right) D_0{}^2 L_e \quad (4.7)$$

Where $\boldsymbol{L_e}$ is the effective length in axial direction for AFPM machine, $\boldsymbol{K_{\emptyset} = 0}$ is the ratio of electrical loading on rotor and stator in a no armature winding machine topology, $\boldsymbol{K_L}$ is the co-efficient considering the factor of temperature rise, losses and design specifications (S Huang et al., 1997; Surong Huang et al., 1998). The total power density of AFPM machine is defined as;

$$P_{den} = \frac{P_{out}}{\frac{\pi}{4} D_{tot}{}^2 L_{tot}} \quad (4.8)$$

Where D_{tot} is the machine`s total outer diameter and L_{tot} is the machine total axial length. This generalized sizing equation in equation (4.7) can be easily applied to any AFPM machine or generator (Dubois et al., 2000; Li & Chen, 2008). The outer diameter surface diameter D_o can be derived as;

$$D_o = \sqrt[3]{\frac{P_{out}}{\frac{\pi \mathrm{m}}{4m_1} K_e K_p K_i A B_g \eta \frac{f}{P} (1-\lambda^2)(1+\lambda)}} \quad (4.9)$$

The outer diameter D_o of the AFPM machine is obtained from;

$$D_{tot} = D_0 + 2W_{cu} \quad (4.10)$$

Where W_{cu} is the end-winding protrusion from the center iron stack in radial direction for radial-flux machine. It is derived as;

$$W_{cu} = \frac{D_i - \sqrt{D_i{}^2 - \frac{2AD_{ave}}{K_{cu} J_s}}}{2} \quad (4.11)$$

Where D_{ave} is the average diameter, J_s is the current density and K_{cu} is the copper fill factor of the bobbin/stator yoke. The machine axial length L_e is given by;

$$L_e = (L_{cs} + 2L_{ss}) + 2L_r + 2g \tag{4.12}$$

Where g is the air gap length, L_r is the rotor axial length. $(L_{cs} + 2L_{ss})$ is the rotor axial length consists of stator core`s axial length and the stator-slot depth L_{ss}. For this particular axial-flux machine design, the L_{ss} = 0. The derivative for L_{cs} is given by;

$$L_{cs} = \frac{B_g \pi \alpha_p D_0 (1 + \lambda)}{4pB_{cs}} \tag{4.13}$$

Where B_{cs} is the stator-core flux density and α_p is the ratio of the average air-gap flux density to the peak air-gap flux density. Thus, the axial length of the rotor L_r is defined as;

$$L_r = L_{cr} + L_{pm} \tag{4.14}$$

Where L_{pm} is the PM thickness. The axial length of the rotor core L_{cr} is defined as;

$$L_{cr} = \frac{B_u \pi D_0 (1 + \lambda)}{8pB_{cr}} \tag{4.15}$$

Where B_{cr} is the rotor disc flux density, B_u is the PM surface flux density. The PM length L_{pm} can be calculated as;

$$L_{PM} = \frac{\mu_r B_g}{B_r - \left(\frac{K_f}{K_d} B_g\right)} K_c g \tag{4.16}$$

Where μ_r is the PM recoil relative permeability. B_r is the PM residual flux density. K_d is the leakage flux factor. $K_f = B_{gpk} / B_g$ is the peak-value corrected factor of the air-gap flux density in the AFPM machine radial direction and K_c is the Carter

factor. The Carter factor can be expressed as (Binns, 1964; Chalmers & Spooner, 1999; Hesse, 1992; A Mahmoudi, Rahim, & Hew, 2011);

$$K_c = \frac{t}{t - \gamma g}, \qquad \gamma = \frac{4}{\pi}\left[\frac{W_{so}}{2g}\tan^{-1}\left(\frac{W_{so}}{2g}\right) - \ln\sqrt{1 + \left(\frac{W_{so}}{2g}\right)^2}\right] \tag{4.17}$$

Where t, γ and W_{so} being the tooth pitch, average slot-pitch and slot opening respectively (Park, Koo, Jang, Choi, & You, 2015).

4.4 Losses and Efficiency

In order to compute the efficiency of electric machine, it is important to probe all losses in the machine. Hence, the machine efficiency can be assessed as;

$$\eta = \frac{P_{out}}{P_{out} + P_{mech} + P_{cu} + P_{eddy\_cu} + P_{core}} \tag{4.18}$$

Where P_{out}, P_{mech}, P_{cu} and P_{eddy_cu}, P_{core} are the output power, rotational loss, copper loss, Eddy current loss due to static high frequency and high frequency magnetic field and core loss respectively (Amin Mahmoudi et al., 2013; Parviainen et al., 2004; Qu & Lipo, 2003; Sadeghierad, Darabi, Lesani, & Monsef, 2010; Virtič & Avsec, 2011). Rotational/Mechanical loss can be calculated from (Hosseini et al., 2008);

$$P_{mech} = \frac{1}{2} C_f \mathcal{P} (\pi n)^3 \left({D_0}^5 - {D_i}^5\right) \tag{4.19}$$

Where $\mathcal{P}$ is the density of rotating part, C_f is the friction coefficient, D_0 is the outer diameter of the surface rotor, n is the rotor speed in rpm. Copper loss and Eddy current losses can be calculated from the following expressions;

$$P_{cu} = R_s \times |I_{load}|^2 \tag{4.20}$$

$$P_{eddy\_cu} = \frac{\left(B_g 2\pi f D_{strand} \times 10^{-3}\right)^2}{32 P_{cu}} \times V_{cu} \quad (4.21)$$

Where R_s is the stator resistance which relates to winding temperature and load. I_{load} is the full load current of machine. f is the rotor frequency, B_g is the air gap flux density, D_{strand} is the diameter of each wire of conductor and V_{cu} is the volume of copper winding. The core loss is expressed as;

$$P_{core} = P_h + P_{eddy\_cu} \quad (4.22)$$

Where P_h is hysteresis loss and P_e is the Eddy current loss. A paper by Atallah *at el*. shows that Eddy current losses may also appear in the rotor disc under the permanent magnets. Since the fundamental air-gap field usually rotates in synchronism with the rotor and the time harmonics in the current waveform and space harmonics in the winding distribution are generally small. Therefore, these Eddy current loss components are usually neglected (Atallah, Howe, Mellor, & Stone, 2000).

4.5 Fitness Function

In optimization process, selection of proper fitness function is very important for obtaining the best solution for a multi-objective problem (Rashtchi, Rahimpour, & Fotoohabadi, 2011). A wrong selection of fitness function may result an inaccurate outcome hence it is essential to fully understand the parameters that are to be studied. In addition, if the GA optimization produces better genes than previous genes repeatedly, the solution may lead towards a local optimum (Açıkbaş & Söylemez, 2008). Hence, this problem can be overcome by incorporating a hybrid optimization or simulate with a larger population for computation. For this AFPM generator machine, equation (4.8) is selected as one of the fitness function for the hybrid optimization tool.

4.6 Genetic Algorithm (GA)

GA is a meta-heuristic search that is inspired by the process of natural evolution which generates solutions to optimization problem. It utilizes processes such as mutation, selection, crossover and inheritance (Xu, Zeng, Liu, & Wang, 2014). In advantage, GA is neither depend on the starting point of the function searches nor require any information of the fitness function/constraint function. Often GA searches for global optima rather than local optima of a fitness function. Since GA does evolve candidate parameters in a population, each candidate is coded as a long binary string of "0" and "1" which is called the chromosome representation. The chromosome is decoded and evaluated of its` fitness performance using a performance function in the optimization tool. For example in optimizing an AFPM generator, the chromosomes of this optimization model are $\boldsymbol{N_{ph}}$, $\boldsymbol{B_g}$, $\boldsymbol{A}$, $\boldsymbol{g}$, $\boldsymbol{P_{out}}$, $\boldsymbol{E_{pk}}$, $\boldsymbol{I_{pk}}$, $\boldsymbol{\lambda}$, $\boldsymbol{\eta}$, $\boldsymbol{D_0}$, $\boldsymbol{L_e}$. After an evaluation is complete, a random generator randomly chooses multiple pairs of higher-quality chromosome to perform subsequent GA evaluation called the crossover and mutation. Upon multiple crossover and mutation evaluation, the weaker chromosomes previously selected are replaced by the stronger chromosomes in the current generation until the set stopping criteria are reached (Montazeri-Gh, Poursamad, & Ghalichi, 2006). With some improvements by the genetic operators, the real-coded GA obtained a better fitness solution than the binary coded GA for a continuous problems.

4.6.1 Chromosome

Genes are the variables that affect the fitness value of the objective function, several parameters are interdependent for an optimal AFPM machine. The chromosomes in this proposed optimization are N_{ph}, B_g, λ, A, g, P_{out}, E_p, I_p, η, D_0, L_e. They are the number of winding turns per phase, flux density in the air gap, diameter

ratio, air gap length, total output power, peaks of phase EMF, peaks of phase current, machine efficiency, outer surface diameter and machine axial length.

4.6.2 Crossover

In crossover, a crossover operator of a real-coded GA is defined by the concept of linear combination of vectors from area of convex set theory (Kao & Zahara, 2008). In this case, a population of 100 to 1000 in every generation has been set and the crossover operator functions to produce next generation child by combining two individuals chosen from the present population. This is usually done with a predefined value of probability set to produce next generation chromosomes so it randomly improves itself. With given probability to produce offspring. Options available are single-point, double-point and shuffle crossover (Cao & Wu, 1999; Dao et al., 2016). In the process of gene selection, optimization methods available include the roulette wheel (random generator), elitist selection and tournament. In this case of scattered crossover, the elitist method is chosen. Two random chromosomes where the genes vector is a 1 from the first parents and genes where the vector is a 0 from the second parent are intervened and the genes are combined to form the new child. Finally, the equivalent sections are exchanged as example below;

Parent-1 = [$\boldsymbol{N_{ph}}$, $\boldsymbol{B_g}$, $\boldsymbol{\lambda}$, $\boldsymbol{A}$, $\boldsymbol{g}$, $\boldsymbol{P_{out}}$, $\boldsymbol{E_p}$, $\boldsymbol{I_p}$, $\boldsymbol{\eta}$, $\boldsymbol{D_0}$, $\boldsymbol{L_e}$]

Parent-2 = [$\boldsymbol{N_{ph}}$`, $\boldsymbol{B_g}$`, $\boldsymbol{\lambda}$`, $\boldsymbol{A}$`, $\boldsymbol{g}$`, $\boldsymbol{P_{out}}$`, $\boldsymbol{E_p}$`, $\boldsymbol{I_p}$`, $\boldsymbol{\eta}$`, $\boldsymbol{D_0}$`, $\boldsymbol{L_e}$`]

the function produces the following child/offspring;

child-1 = [$\boldsymbol{N_{ph}}$`, $\boldsymbol{B_g}$, $\boldsymbol{\lambda}$`, $\boldsymbol{A}$`, $\boldsymbol{g}$, $\boldsymbol{P_{out}}$`, $\boldsymbol{E_p}$, $\boldsymbol{I_p}$, $\boldsymbol{\eta}$`, $\boldsymbol{D_0}$`, $\boldsymbol{L_e}$]

4.6.3 Mutation

Random mutation operator for real-coded GA operates on the gene by introducing it into a perturbation in a random number range between 0-1 in the feature`s domain. In general context, mutations function specifies how GA incurs minor random alteration in individual chromosome in a population to obtain mutated children. Mutation in GA enables diversification to search in wider region of function spaces. By default, a probability in between 0.005 to 0.05 is assigned in the process and a new random real coded chromosome is produced at the end of process. In real coding, random value is chosen among genes from the probability interval. Subsequently, the newly selected random values replace old values in the genes pool (Raajan, Bharanikumar, Bhuvaneswari, & Subramanian, 2015).

4.7 Pattern Search Tool (PS)

Traditional optimization methods use information about gradient of a derivative to search for an optimal point by looking for best fitted value among a set of points in a region. As opposed to that, Pattern Search solves a given optimization problem without the need to acquire information gradient of the objective function (Güneş & Tokan, 2011). Pattern Search tool is also known as “Direct Search Algorithm” that searches a pool of points around the current points (Amrita & Mohan Rao, 2011). This method can solve problem for any non-differentiable or even continuous objective function, and it works by computing a number of points that get comparatively close to the optimal point. In this process, the tool searches a pool of points called a “mesh” around the current points (the points computed in the previous step). Next, this algorithm formulates a mesh by adding the current points to a scalar multiple of a fixed set of vectors called pattern (J. Kim & Kasabov, 1999). Upon continuous iteration, the algorithm is terminated if a point in the mesh shown to have improved the

objective/fitness function value of the current point, the newly selected point replaces the current point to be in the next step in the algorithm (Căleanu, Mao, Pradel, Moga, & Xue, 2011; Cao & Wu, 1999; Dao et al., 2016; J.-K. Kim, Cho, Jung, & Lee, 2002).

4.8 Hybrid GA-PS Algorithm

Crossover and mutation is the core of GA, it has better robustness and adaptability into any objective functions interdependent on any constraint function. Besides, the problem involved does not need to be in continuous or differentiable form. As known, GA is best at solving complicated functions and it does not easily fall into local optimum of a fitness function. However, the algorithm occasionally does not converge to the actual depth of the global minimum (Marinakis et al., 2010). So, GA and PS algorithm are combined in order to overcome the above problem.

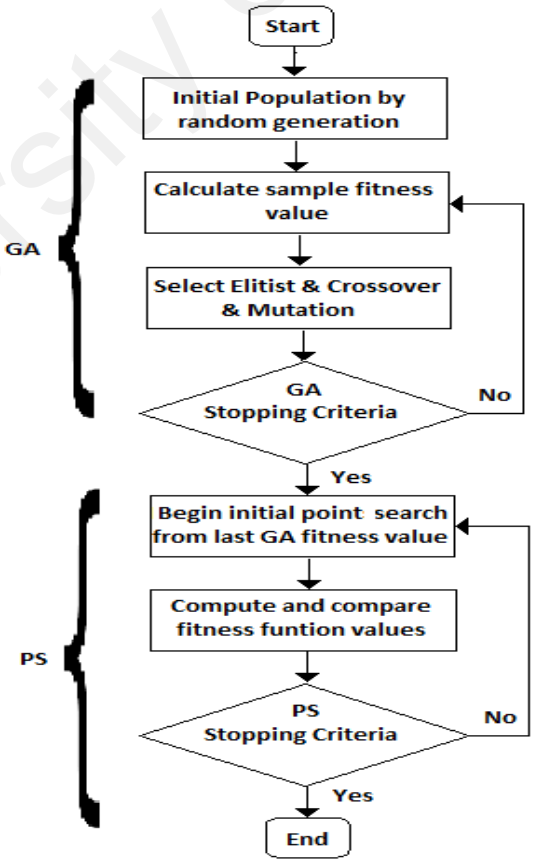

Figure 4.2: Flowchart of GA-PS optimization

In the hybrid model, GA in MATLAB initializes the initial population based on preset generated population and all the candidates are to be vectorized in m × n matrix string, usually is in the form of multiple-column single-row matrix as shown in section "Crossover Operator". Then, the first fitness value based on minimized fitness function variables is calculated and the best fitness value (Elitist) is selected. Followed by crossover, genes from each parent are intervened and the similar number of new child/offspring generation is created. Finally, a small mutation probability ratio is imposed on randomly selected chromosomes. Upon reaching the set stopping criteria, the best value of variables with the best fitness function value is delivered to the next Pattern Search algorithm to perform search computation. In the Pattern Search algorithm, all previously returned values are added to the mesh size in a pattern vector. The algorithm calculates the objective function at mesh points until it spots one which the value is smaller than the previous smallest value (Cao & Wu, 1999; Dao et al., 2016). With a large population, the hybrid GA-PS searches the solution space more thoroughly, thereby confirms the function converges to the global minimum. However, this algorithm runs more slowly with a larger population size subject to preset generation. Although there are multiple tools to perform hybridization, this GA-PS hybrid model is chosen as it could provide more consistent and more accurate best fitness value, it ensures the function converges to the actual depth of the local optimum on the PS mesh pattern. Another reason is because the algorithm is easily accessible in the MathWorks development environment or programmable in other programming language. Figure 4.5 to figure 4.7 show the preliminary comparison result between GA, PS and hybrid GA-PS using the famous "Rosenbrock`s" test function (Juang, 2004). It is shown that the best possible solution obtained is by the hybrid GA-PS algorithm, the best fitness value is $8.765 \times 10^{-6}$ which is relatively close to the actual global optimum value of zero of the Rosenbrock`s function as shown in figure 4.4. To implement this

hybrid algorithm into optimizing the AFPM machine, a MATLAB GUI optimization tool was developed that follows the GA-PS optimization process flow as shown in figure 4.3.

Table 4.1: Design restriction and requirements

Rated output power	P_{out}	120W
Inner diameter to outer diameter ratio	λ	$0.4 \leq \lambda \leq 0.75$
Axial-length of generator	L_e	$L_e \leq 100$mm
Air-gap length	g	4.0mm ≤ g ≤ 6.0mm
Stator core flux density	B_{cs}	$< 1.20T$
Rotor flux density	B_{cr}	$< 1.20T$
Permanent remanence	B_{max}	1.30T
Rated line voltage	V_p	≤ 150V
Maximum phase current	I_{rms}	≤ 1A
Air-gap flux density	B_g	$0.5 \leq B_g \leq 1.0$
Electrical loading	A	$1000 \leq A \leq 35000$
Pole pairs	P	4
Efficiency	η	≥ 85%
Frequency	f	65Hz
Number of phases	m	3

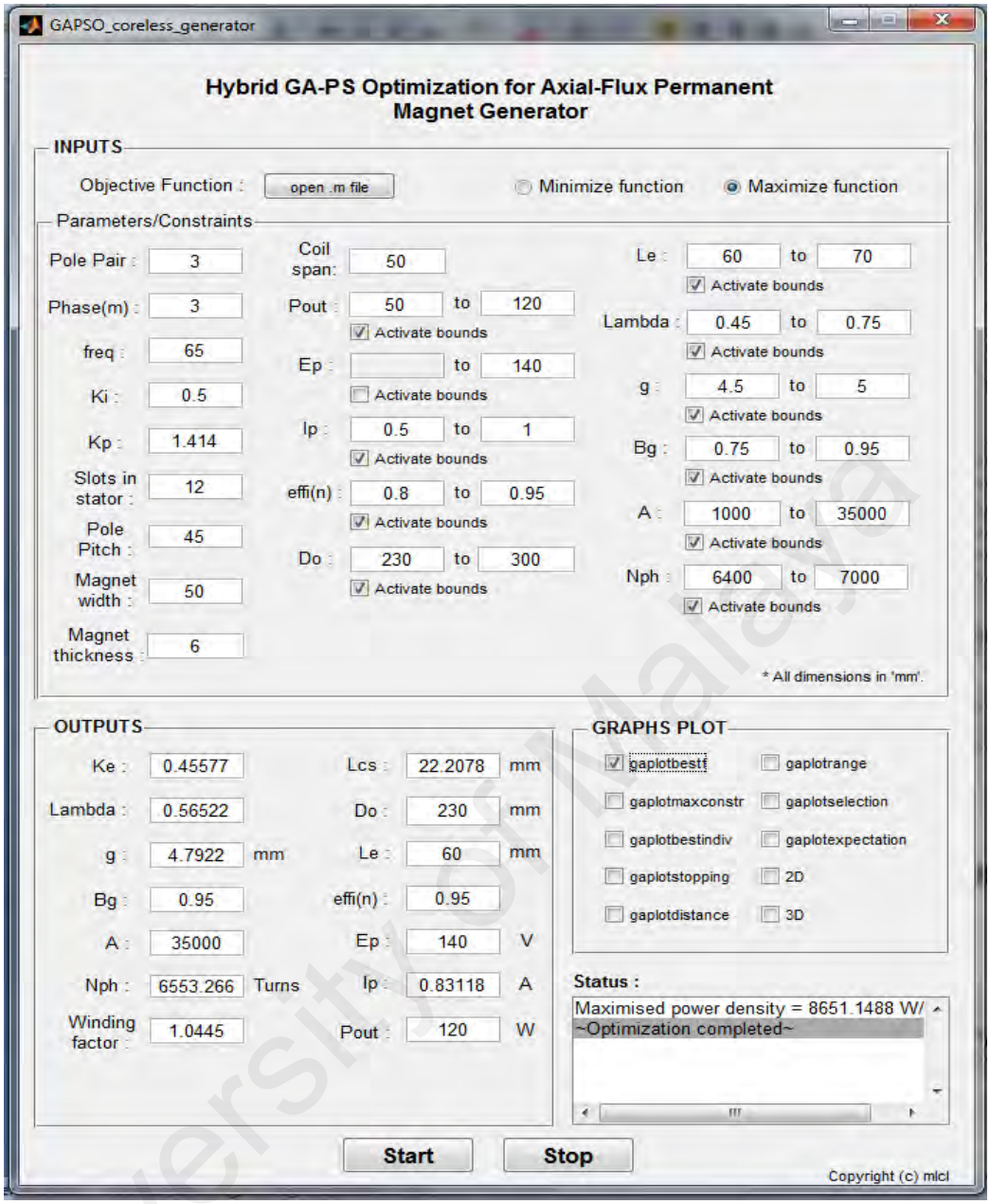

Figure 4.3: GA-PS optimizer developed in MATLAB GUI

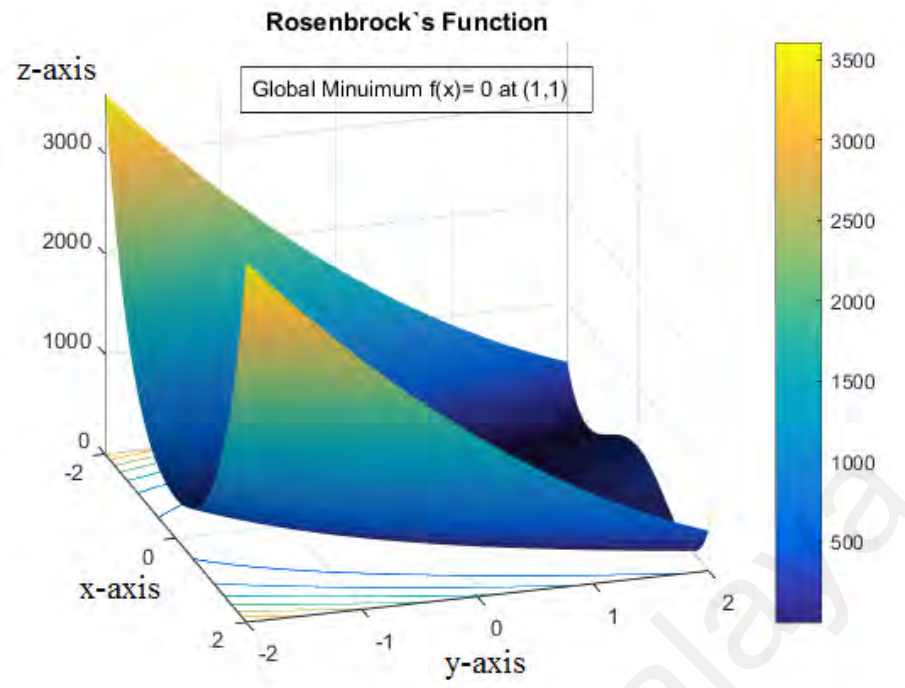

Figure 4.4: Rosenbrock`s wave function.

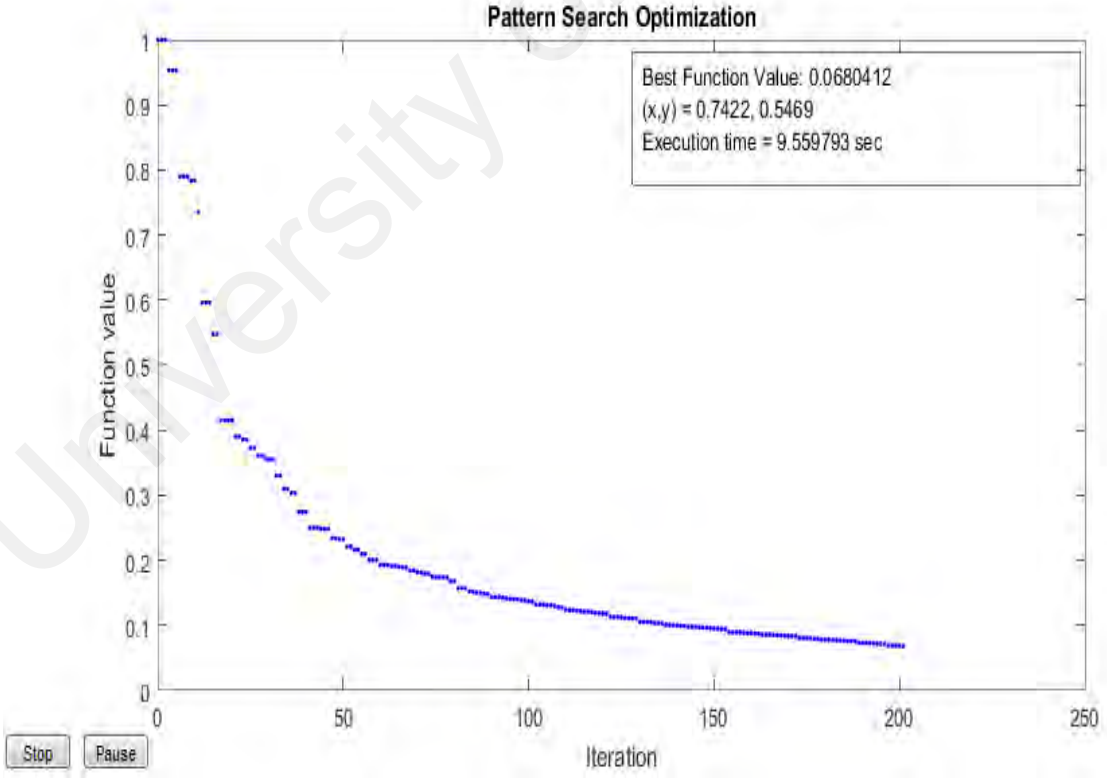

Figure 4.5: Rosenbrock`s test function by Pattern Search.

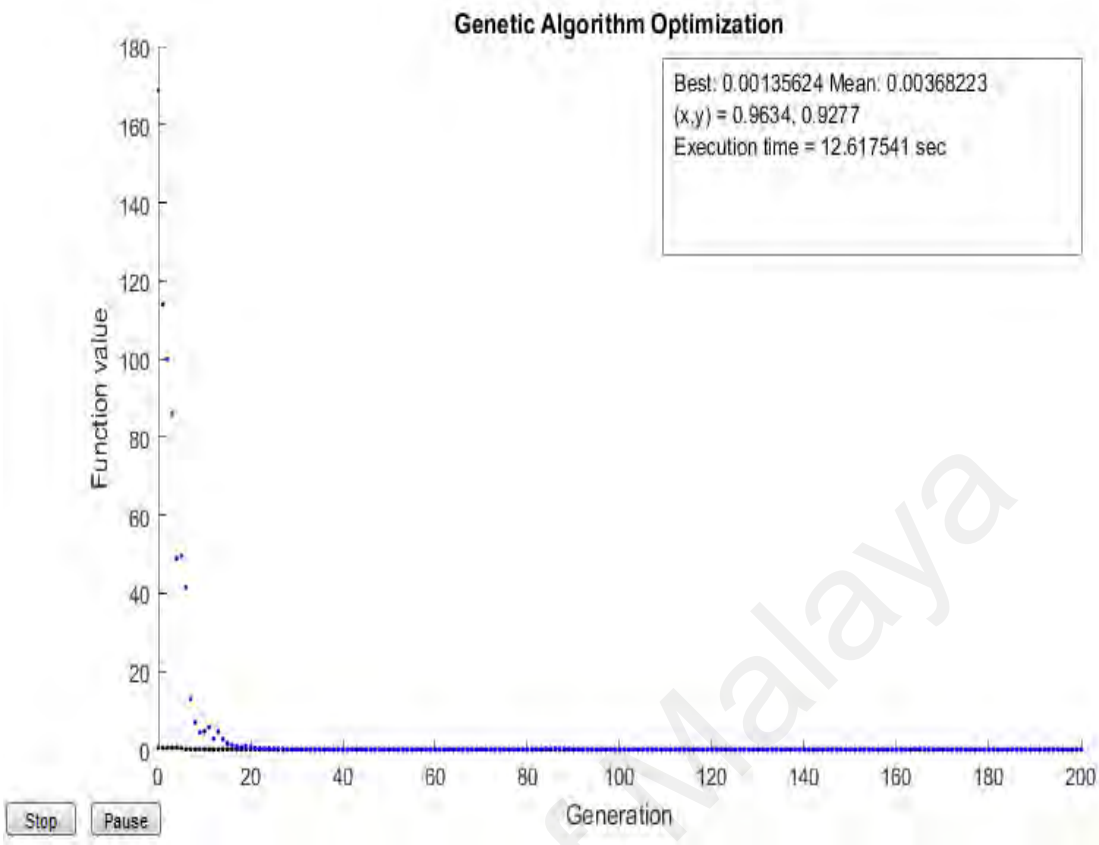

Figure 4.6: Rosenbrock`s test function by Genetic Algorithm.

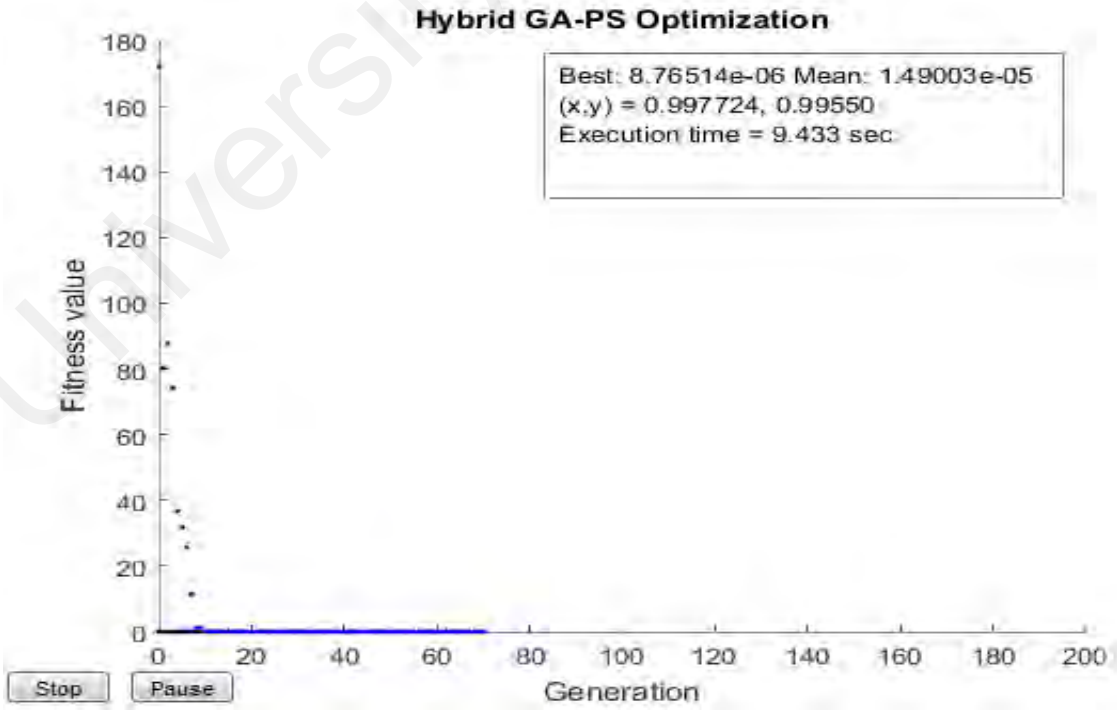

Figure 4.7: Rosenbrock`s test function by hybrid GA-PS.

4.9 Finite Element Analysis (FEA)

Despite the hybrid GA-PSO algorithm has facilitated the process to acquire the maximum power density of the proposed generator. The computed parameters obtained in MATLAB GUI in the optimization tool needed to be further analyzed to validate the practicality. To achieve that, three-dimensional FEA is incorporated to analyze the magnetic flux saturation, to evaluate power density and validate the induced back-EMF during static and dynamic simulation (Chung & You, 2014; Ali Mahmoudi et al., 2013). The FEA software used is the ANSYS 3D Maxwell. Figure 5.2 shows the auto-mesh results of the proposed AFPM generator. The top stator part has been hidden in order to access the mesh pattern of the machine`s rotor. Using symmetrical characteristic of this AFPM generator, a quarter of the design has been split out relative to the vertical axis in axial direction as seen in figure 4.8 and this has drastically reduced the model analysis period. Figure 4.8 shows the exploded model of AFPM generator at the end of the simulation as well as figure 4.9 and figure 4.10 show the magnetic flux path arrows pointing in the direction from magnet pole in air gap and magnetic flux distribution, respectively. As in figure 4.10, the FEA result shows that there is no magnetic material to permeate/guide magnetic flux lines formation thus more losses of magnetic field around the outer circumference of the rotor is expected. The same figure also shows the flux density obtained in FEA transient analysis, the rotor has been captured at 50^{o} rotated out of the phase current coils, it can be seen that around the circumference of each circular permanent magnet indicates the strongest magnetic flux density compared to other part of the rotor. Lastly, that performance prediction of the meshed model and flux density have been obtained and verified by the 3D FEA. Figure 4.11 shows the coil windings with iron-stator core (center) for comparison with AFPM coreless generator.

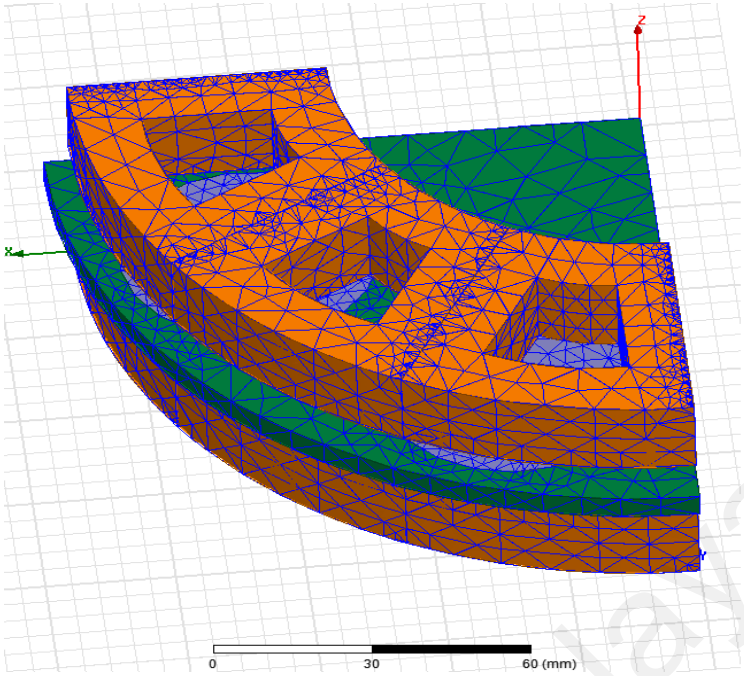

Figure 4.8: Meshed model for one-fourth of the AFPM machine.

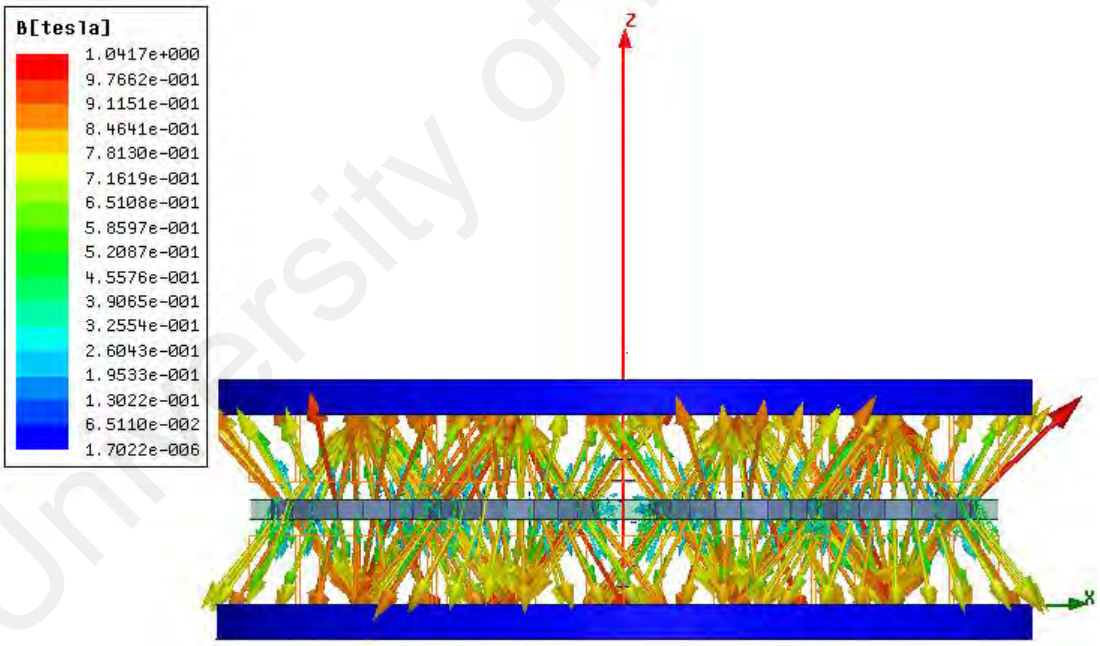

Figure 4.9: Magnetic flux vector distribution obtained by FEA.

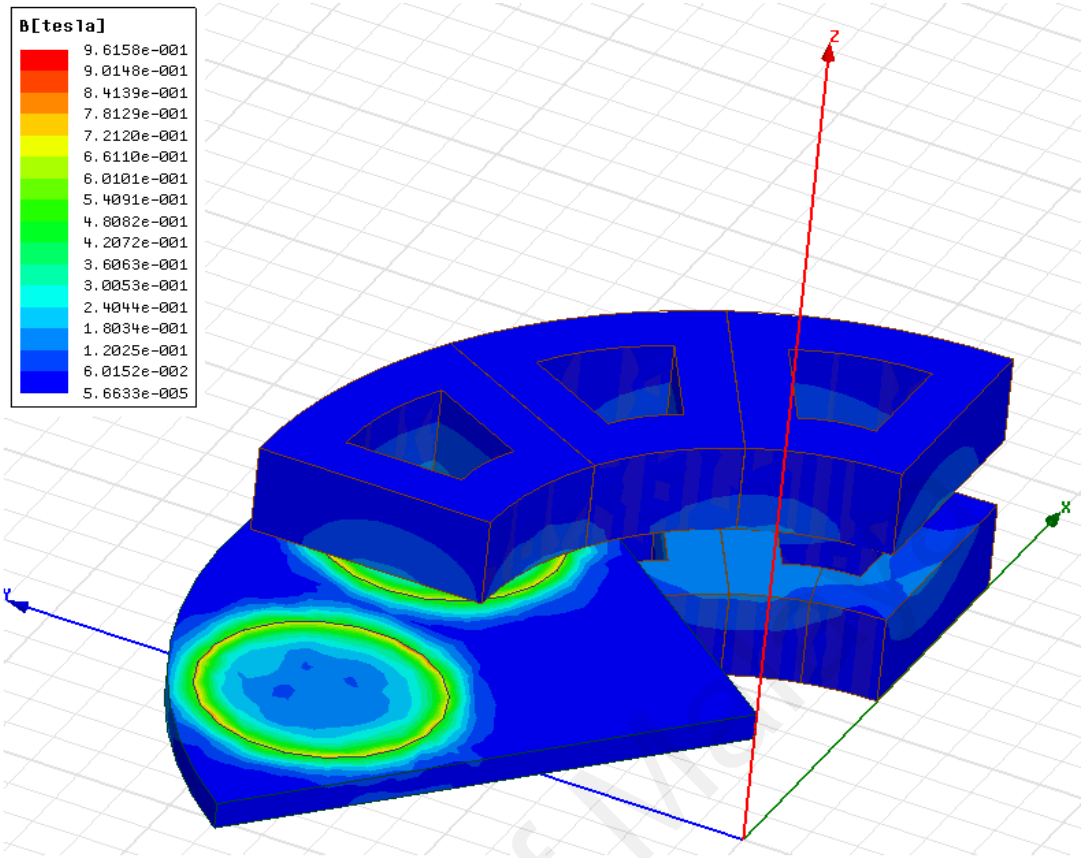

Figure 4.10: CAD design and FEA flux density of the 1/4 model.

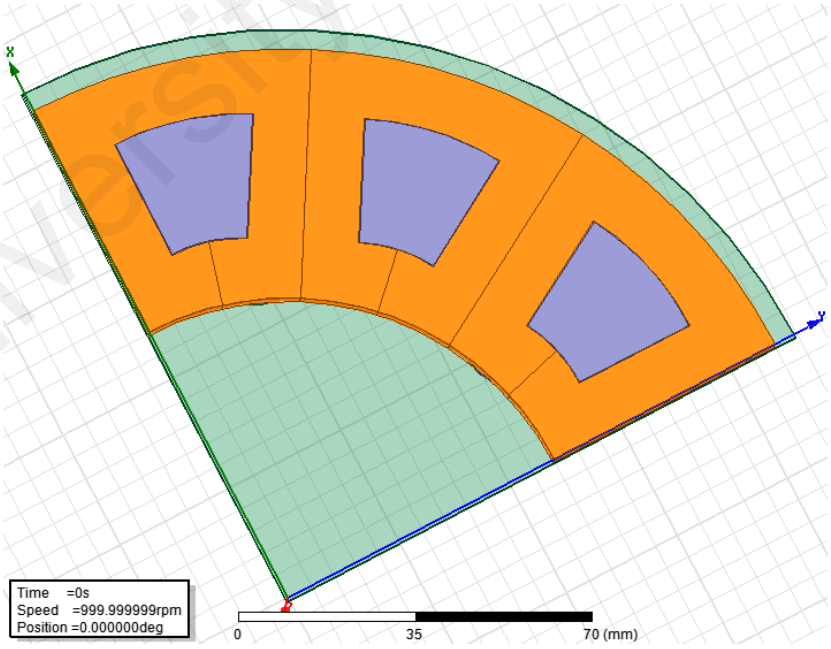

Figure 4.11: Coil windings with iron-stator core (center).

4.10 Final Designs

Figure 4.12 shows the exploded view of a double-stator single-rotor AFPM generator based on design data. The actual generator consists of two stators and one rotor as seen in figure 4.13. With no iron core means reduction in weight and cogging torque. The stator windings are placed 4.5mm physical clearance from the rotor disc at the front and rear side. On both sides of the rotor disc, circular flat shape NdFeB N48 permanent magnets are placed onto an acrylic plexi-glass rotor disc. Solid hard wood back-plates are used as supporting structure for the stator windings. Since the machine body is built with low magnetic permeability material, the magnetic field on the rotor is less sensitive to the flux variations in air-gap. By using non-magnetic material for the armature support structure, this minimizes axial forces between the stators and rotor hence, eliminates cogging torque in the generator. In this AFPM generator, the permanent magnet arrangement (NS) configuration can be seen in section "4.11.3 rotor". Twelve trapezoid bobbin cores made from the ABS plastic and copper coils are wound that forms the concentrated armature coils. These armature coils are then glued onto non-magnetic non-conducting material such as wooden back-plate. One suggested material is the carbon fibers because it is low in weight yet very durable relative to metallic materials, also it is resistive against temperature variation (Javadi & Mirsalim, 2010). Table 4.2 tabulates dimensions and specifications for the proposed generator. These design dimensions and specifications are obtained based on the proposed hybrid GA-PS optimization tool and FEA simulation.

Table 4.2: Design data of proposed machine

Rated output power	P_{out}	120W
Rated RMS voltage at rated 1000 rpm	V_{rms}	$140/\sqrt{2}$
Number of poles	2xP	8
Number of phases	m	3
Number of winding turns per phase	N_{ph}	19500/3
Pole pitch	γ_p	45^o
Air-gap length	g	4.5mm
Outer diameter	D_0	235mm
Inner diameter	D_i	132mm
Magnet thickness	L_{pm}	6mm
Frequency	f	65Hz
Stator-yoke thickness	L_{cs}	20mm
Rotor-yoke thickness	L_{cr}	6mm
Number of stator slots	Q	12
Efficiency	ɳ	95%
Air-gap flux density	B_g	0.75T
Optimized Power density	P_{den}	8651 W/m^3

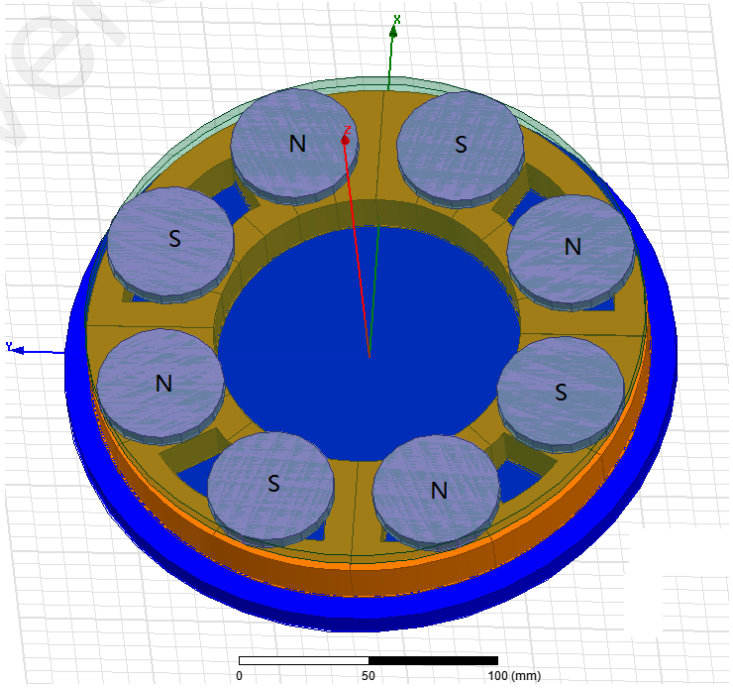

Figure 4.12: Proposed AFPM generator based on design data.

4.11 Machine Construction

Figure 4.13 shows the prototype of 120W, three-phase, 65Hz, 8-pole double-stator single-rotor AFPM generator. In construction, the structure is shaped using the Computer Numerical Control (CNC) machine because this method can improve machine precision and balancing. Less friction equals lower bearing loss, industrial grade bearings are used in the machine to reduce rotor friction. Moreover, parameter such as the air-gap length is studied to produce best result. By using wooden joints, the stators can be fixed in position tightly, the length of the air-gap is thus fixed by using two shaft key lockers on both sides of the rotor.

Figure 4.13: Prototype three-phase AFPM machine.

Figure 4.13 shows the machine stator plates from side view. The stator plate is made from a solid non-ferromagnetic material. It holds the coil windings around the bearing. The bearings are forced into each hole in the middle of stator plate. The rotor shaft is put through the bearing in the prototype machine.

4.11.1 Stator

Winding stator in axial-flux machine is obviously different from those in radial-flux machines. A coreless stator can be any non-ferromagnetic material such as “Teflon”, “Polyurethane” and etc. In order to wind copper wires into individual coil, “ABS” plastic bobbin is used as the stator core, this is because ABS plastic is easily formable and has a material permeability equivalent to vacuum. The core bobbins are printed by 3D printer as the printed material is harder and resistant to high temperature. Figure 4.14 shows four coil windings are placed onto a stator back plate.

Figure 4.14: Coil winding on stator back plate.

The holes on the stator plates are used to position the coils around the axis of rotation. The angle between two holes is 30^{o} to fit in twelve coil windings on each stator back plate.

4.11.2 Winding the Stator

Windings are made manually by using winding machine, figure 4.15 shows a coil winding wound by the machine. These coil windings are arranged circumferentially on the stator plate and they are connected in three-phase wye-connection. To avoid coil windings displaced from their position caused by machine vibration, epoxy glue is

applied to the coil winding in order to reinforce the winding. A special type of high temperature resistant tape was used to cover the winding to avoid short circuit and provide good heat conductivity.

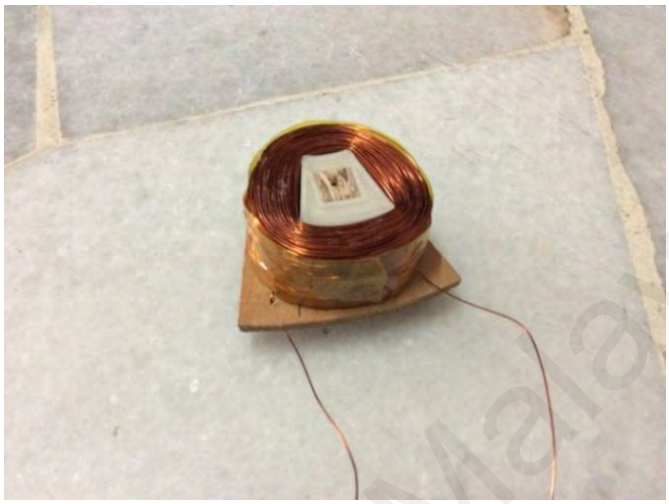

Figure 4.15: Individual stator coil winding.

Figure 4.16: Windings configuration for 12-stator core count.

4.11.3 Rotor

To eliminate magnetic flux reluctance inside an iron rotor, acrylic sheet is selected as the rotor material. The rotor is fabricated by the CNC machine. First, two circular discs with 240mm diameter are cut from a large 5mm thick acrylic sheet. Then,

the discs are brushed by grinder tip to perfect circular. Eight dented holes are milled from the disc surface followed by permanent magnets are glued into each dented fix holes. The two discs with mounted permanent magnets are glued together to form a solid 10mm thick rotor disc shown in figure 4.17.

Figure 4.17: Eight-pole single-rotor double-stator assembly.

Figure 4.18: Rotor disc with 8 permanent magnets.

To fix the rotor disc to a shaft, shaft collar is used. Figure 4.18 shows the constructed rotor disc with eight permanent magnets, each magnet is placed in opposite polarity to its adjacent permanent magnet.

4.11.4 Permanent Magnet

Rare earth Neodymium Iron Boron (NdFeB) permanent magnet is very cheap and easily available in the market. This type of permanent magnet was first used in 1980s. In the prototype machine, circular NdFeB permanent magnet grade N48 is used. The reason is this type of permanent magnets has highest magnetic density compared with other kinds of permanent magnet. The magnetic force can be increased and reduced according to different cutting proportion of the magnet. With the strength of small size, light weight and strong magnetic force, Neodymium magnet is the best price performance magnet available. Figure 4.18 shows the permanent magnets mounted on rotor disc.

Figure 4.19: Variety of magnets used in permanent magnet machine.

4.11.5 Experiment Setup

This section illuminates the testing procedure and the performance aspect of the generator. An experiment is set up to test the performance of the prototype generator.

Figure 4.21 shows the hardware schematic for the experiment setup. In the experiment, the back-EMF, Eddy current losses, cogging torque and output power are the main performance parameters to be studied.

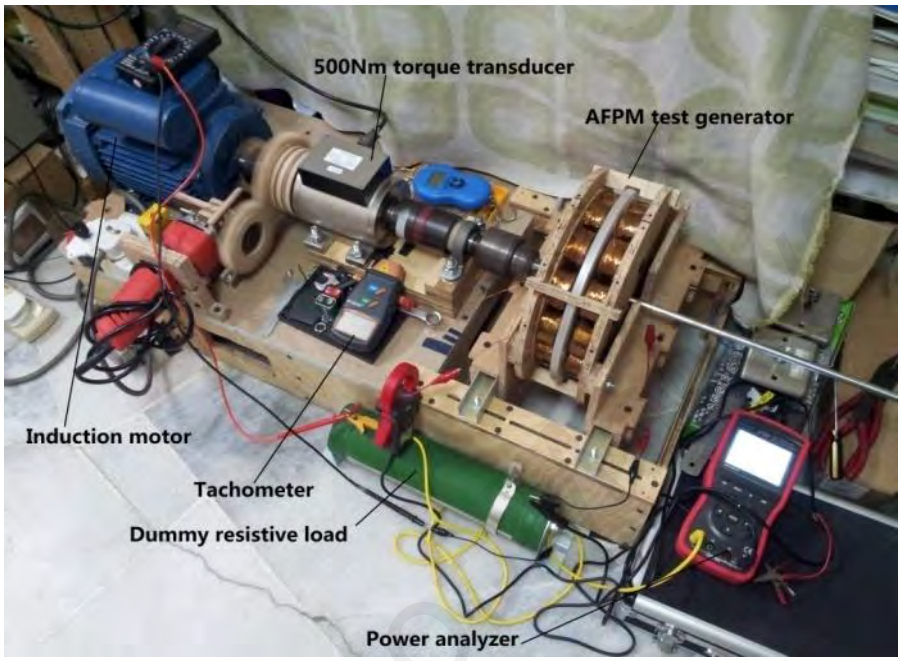

Figure 4.20: Hardware setup of experiment test bench.

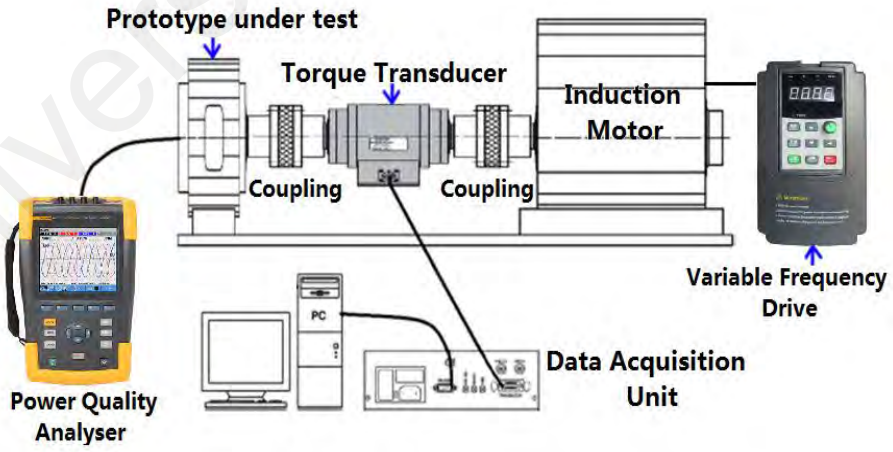

Figure 4.21: Hardware schematics of prototype generator.

The designed prototype generator is mechanically coupled to a 1.5kW induction motor used as prime mover, a torque transducer is connected between the prototype

generator and the prime mover/motor. The rotational speed of the prime mover is controlled using a variable frequency drive (VFD). The NI USB-6009 DAQ unit is used to acquire data from torque sensor, “ETCR 4700” power analyzer is used to measure the output power from prototype generator. The torque in the generator is recorded through the torque transducer with accuracy of ±5%. Three-phase variable high power resistors are connected to the prototype terminals in wye-connection in order to simulate electrical loads. As the load resistance is varied, the loading of the test generator varies hence enables speed-torque characteristic and voltage-current characteristic of the designed generator to be precisely measured. An IR temperature instrument is also used to record the temperature of the armature coils.

CHAPTER 5: RESULTS AND DISCUSSION

5.1 Introduction

Machine design, optimization and simulation based performance evaluation were assessed in previous chapters. Then, the optimized AFPM generator was fabricated. In order to avoid mechanical failure and to achieve the desired characteristic, the mechanical parts should be fabricated precisely as designed. This chapter presents the test results of the prototype AFPM generator.

5.2 Optimization Results

Among the results obtained by using PS, GA and hybrid GA-PS in MATLAB, a more consistent and better accurate fitness value obtained in the hybrid GA-PS model. As seen in figure 5.1(a), the optimized machine`s maximum power density is computed based on the objective function in equation (4.7) to equation (4.9) subject to several constraints in table 4.1. The maximum power density computed by using hybrid GA-PS is at 8651 W/m^3 and the value remains constant throughout the population from 100 to 1000, GA-based calculated power density fluctuates between 8548 W/m^3 to 8651 W/m^3 within the same population range, this clearly shows that GA does not converge to the actual global optima thus giving less accurate best fitness value at low population size. The worst result of fitness value is obtained in PS, the power density fluctuates between 9534 W/m^3 to 7851 W/m^3. In figure 5.1(b), the computed maximum constraint value for hybrid GA-PS is 1.474×10^{-8} regardless of the number of population size. However, PS and GA show a drastic decline of maximum constraint value as the population size increases.

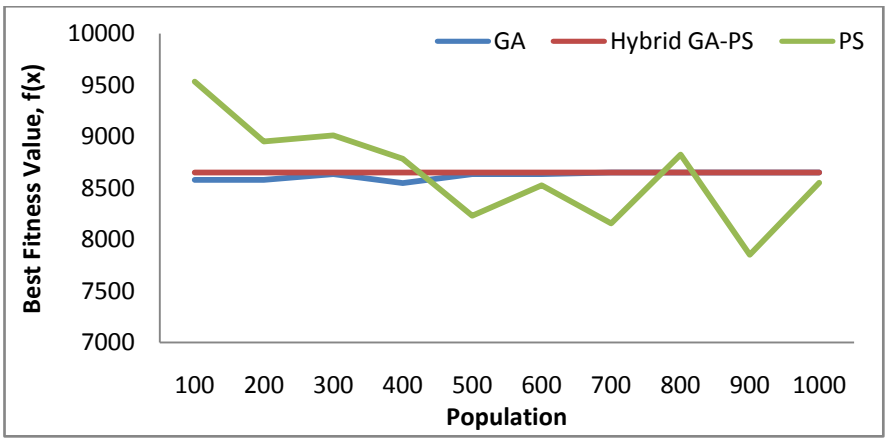

(a)

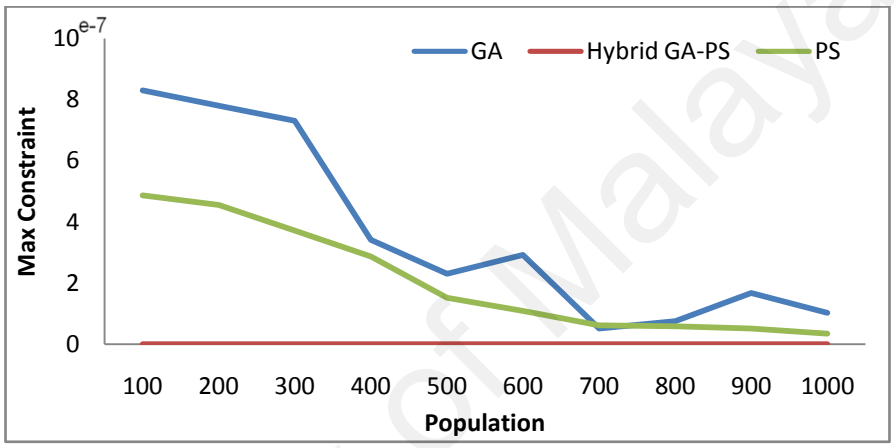

(b)

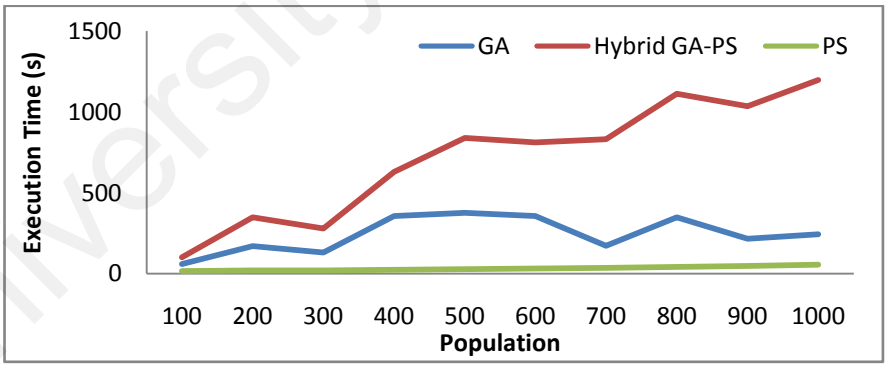

(c)

Figure 5.1: (a) Fitness value versus population. (b) Maximum constraint versus population. (c) Execution time versus population.

For comparison of execution time in figure 5.1(c), result shows that the hybrid GA-PS has a convergence rate that is relatively slower compared to PS and GA. It can be seen that in order for the hybrid GA-PS to converge to the actual depth of the local

optimum, the time taken for computation increases two to three fold. As the population size increases, the convergence rate for hybrid GA-PS increases. On the other hand, PS shows a better convergence rate at average execution time of 31.8 seconds within 1000 population. In conclusion, the overall performance of hybrid GA-PS model shows a better outcome in optimization method for this research particularly at lower population size. Unlike GA and PS, population size has only minor effect in the hybrid GA-PS on local optimum search. For instance, the hybrid GA-PS has obtained a very consistent fitness value even though when the population size is only as low as 100.

5.3 Simulation Results

Figure 4.8 shows the one-fourth of the designed generator in FEA simulation. Figure 5.2 shows the exploded 3D model that is meshed with tetrahedral elements, it can be seen the meshes are more confined around the edges of the circular permanent magnets because this can produce more accurate analysis results. Figure 5.3 shows the air-gap flux density distribution between the permanent magnet and stator coil surface in the AFPM generator, the highest value obtained is 550mT at 50mm along the axis of rotation. Magnetic flux density evaluation is essential to detect any saturation effect on any part of the design structure. It can also evaluate other parameters of the AFPM generator more accurately.

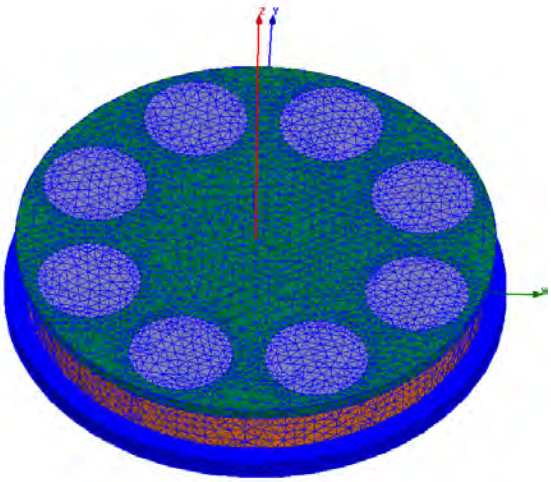

Figure 5.2: Field analysis of three-dimensional auto-mesh generation.

Figure 5.3: Magnetic flux density distribution of the air gap for average radius.

5.3.1 Back-EMF Waveform

One particular research objective is to design the AFPM generator with most sinusoidal back-EMF waveform. Figure 5.4 depicts the generator three-phase back-EMF sinusoidal waveform obtained at 1000 rpm. In the figure, one complete wave cycle measured at peak to peak is 18ms to 33ms, the frequency is calculated to be about 66.66Hz. At 65Hz, the simulation back-EMF peak value is 149.47V which is 6% higher

than the peak back-EMF value obtained in experiment. This is because the losses due to friction and Eddy current exist in experiment while these losses are not considered in simulation.

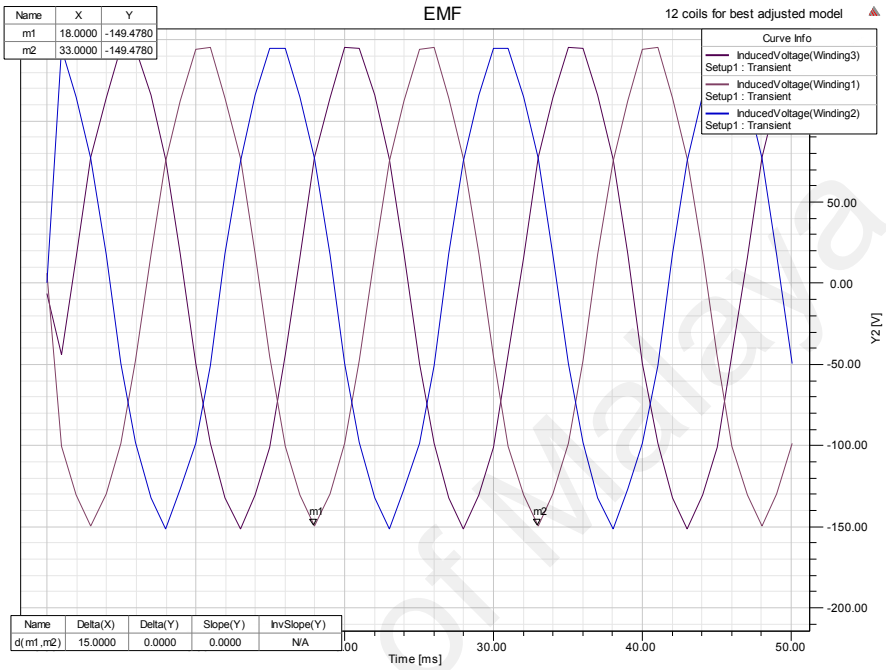

Figure 5.4: back-EMF in FEA.

5.3.2 Eddy Current Losses

To determine the no-load losses, no-load tests were carried out on the generator. The major losses that occur are the windings Eddy current losses and bearing losses (Nguyen, Tseng, Zhang, & Nguyen, 2011). Figure 5.5 shows the no-load losses versus speed plot between experiment and simulation based on equation (4.19) to equation (4.21). Results are clear that the major component of the no-load losses in this generator is attributed to the shaft bearing. For instance, bearing losses occupy about 83% in the total no-load losses at 1000 rpm. In the same figure, Eddy current losses in stator windings are less significant compared to bearing losses even though the rotational speed reaches 1000 rpm. This result has shown that good less-friction shaft bearing used in rotating machine can improve performance of the generator (Muljadi et al., 1999b).

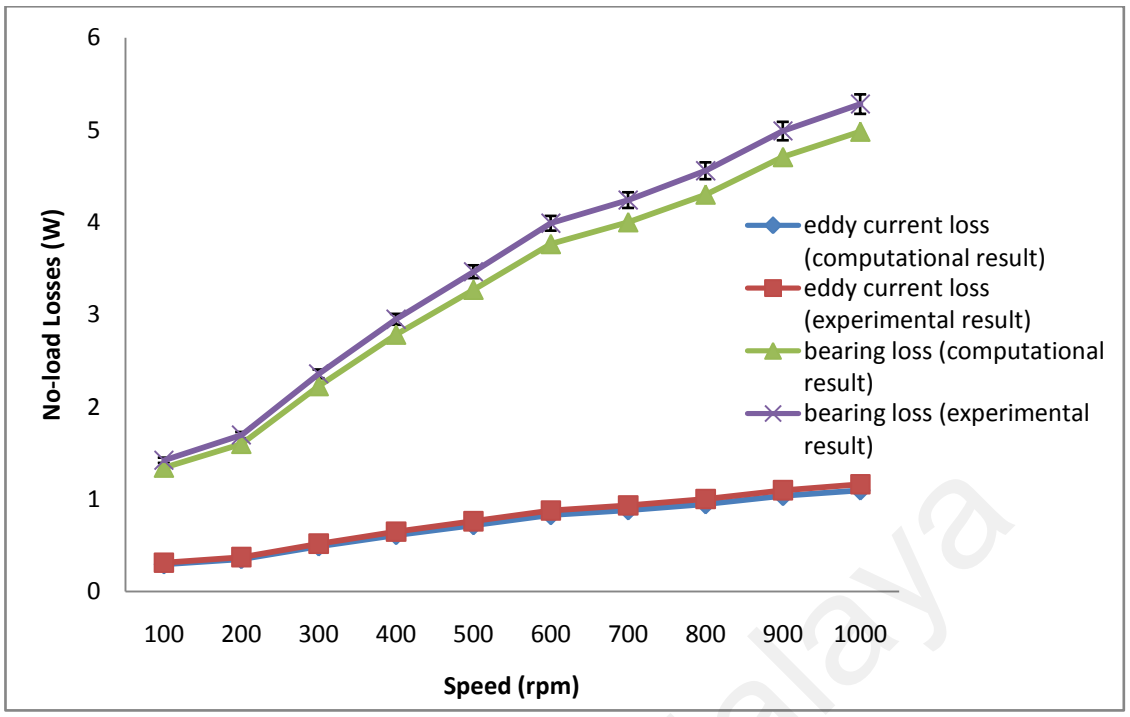

Figure 5.5: No-load losses versus speed.

5.3.3 Cogging Torque

To compare the no-load cogging torque, a coreless-stator core design in figure 4.8 and an iron-stator core design in figure 4.11 are compared in 3D FEA. Figure 5.6 shows the comparison of no-load cogging torque in iron-core and ironless stator based on the proposed APFM generator. The peak value of cogging torque is ± 0.252 Nm for the ironless (coreless) AFPM generator while the iron core configuration is ± 1.328 Nm. Using the air-gap flux density distribution described in equation (3.14) to equation (3.19), the cogging torque is computed from FEA simulation. Since this coreless generator is mainly fabricated from non-ferromagnetic material such as laminated wood and plastic, the armature reaction in ironless stators is insignificant due to very small cogging torque in the generator. By comparison, it is clear that the cogging torque in a coreless stator AFPM generator is significantly lower by approximately 5 times than the AFPM generator with iron-stator core. Hence, lower cogging torque increases electric machine efficiency (Islam, Islam, Sebastian, Chandy, & Ozsoylu, 2011).

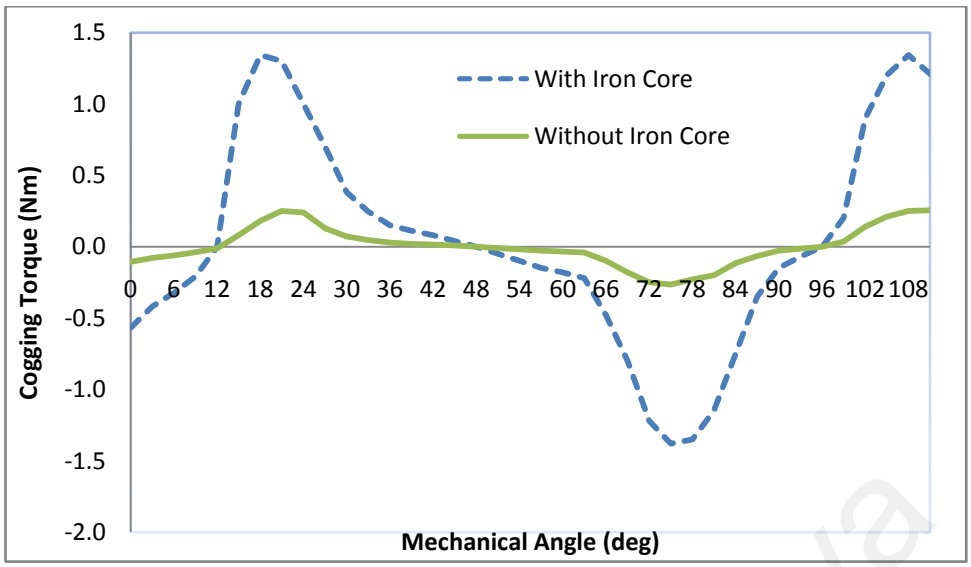

Figure 5.6: Cogging torque between the iron-stator core and air-core stator of AFPM generator.

5.4 Experiment Results

Experiments were set up to test the prototype AFPM coreless generator as shown in figure 4.20. The experiments include the no-load test, load test, output power, speed-torque acquisition, speed-temperature acquisition and efficiency measurement. Performance tests on the prototype AFPM generator were carried out in laboratory. The results obtained are the terminal voltage, output power, power density, torque and machine efficiency. A network of high power adjustable resistors was connected across the AFPM generator terminals in Star-Delta (wye-delta) connection. Simulation results and experiment results are compared and discussed.

5.4.1 Back-EMF Measurement

Figure 5.4 depicts the generator three phase back-EMF sinusoidal waveform at 1000 rpm. At 65Hz, the measured back-EMF peak value is 140V which is lower than the peak back-EMF value by 6% as shown in figure 5.7. Figure 5.8 displays the plot of output voltage versus rotational speed (rpm), the plot shows the terminal voltage is

proportional to rotational speed, hence, the generator produces higher terminal voltage as the rotational speed increases. Throughout the rotational speed from 0 rpm to 1000 rpm, the maximum percentage voltage regulation is about 7% between experimental result and computational result.

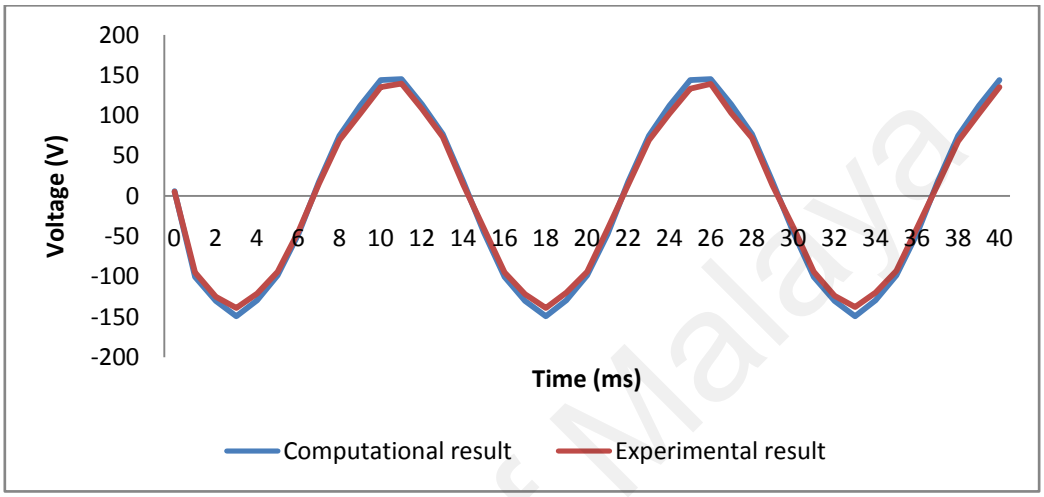

Figure 5.7: Measured back-EMF waveform of the AFPM prototype.

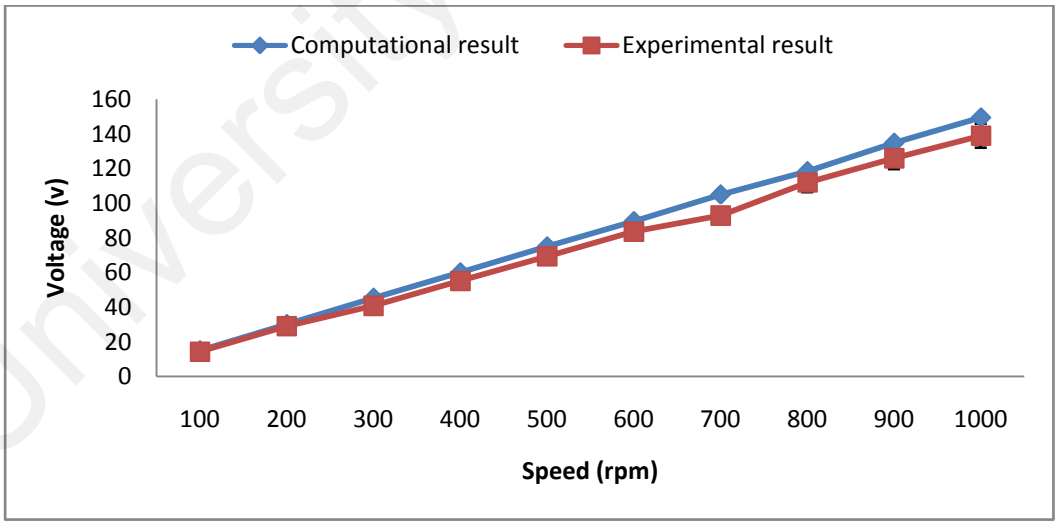

Figure 5.8: No load back-EMF versus speed.

5.4.2 Load Test Measurement

In load test, it is carried out using variable resistive loads; the load resistance are set at 20 Ohm, 60 Ohm and 100 Ohm respectively while the generator speed is kept

constant to measure the output power characteristics. Figure 5.9 shows the output power comparison for the three load resistance values. From the result, it is clear that the load resistance is proportional to rotational speed. The higher the load resistance, higher the output power is produced. For instance, for the load resistance 100 Ohm at 1000 rpm, the measured output power is about 5% less than the predicted output power due to losses in the bearing friction, and Eddy current losses.

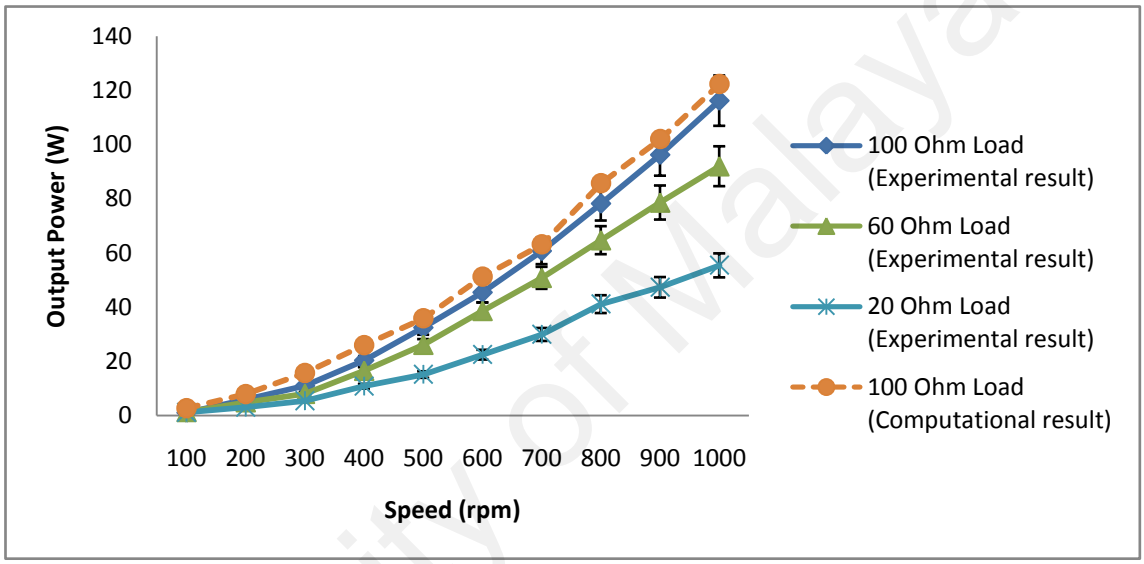

Figure 5.9: Output power versus speed.

5.4.3 Cogging Torque

A network of resistive loads is connected to generator terminals to simulate load condition in order to measure the speed-torque characteristics. Figure 5.10 shows the speed-torque characteristics comparison between simulation and experiment at different resistive load values. For instance at 1000 rpm, the measured torque at load 100 Ohm is lower than the predicted torque value by 0.06 Nm. The speed-torque characteristic is approximately linear. As seen in figure 5.10, the predicted torque and measured torque at 100 Ohm has discrepancy about 0.1 to 0.2 Nm. This is because in experiment, there is resistive loss which causes the temperature of stator coils to raise hence further

increases the resistance in the windings that resulted in lower current flow (Sadeghierad, Lesani, Monsef, & Darabi, 2009b). Therefore, a larger diameter conductor wire can be used to increase the conductivity of current. In addition, fan cooling can be another conventional solution to this problem.

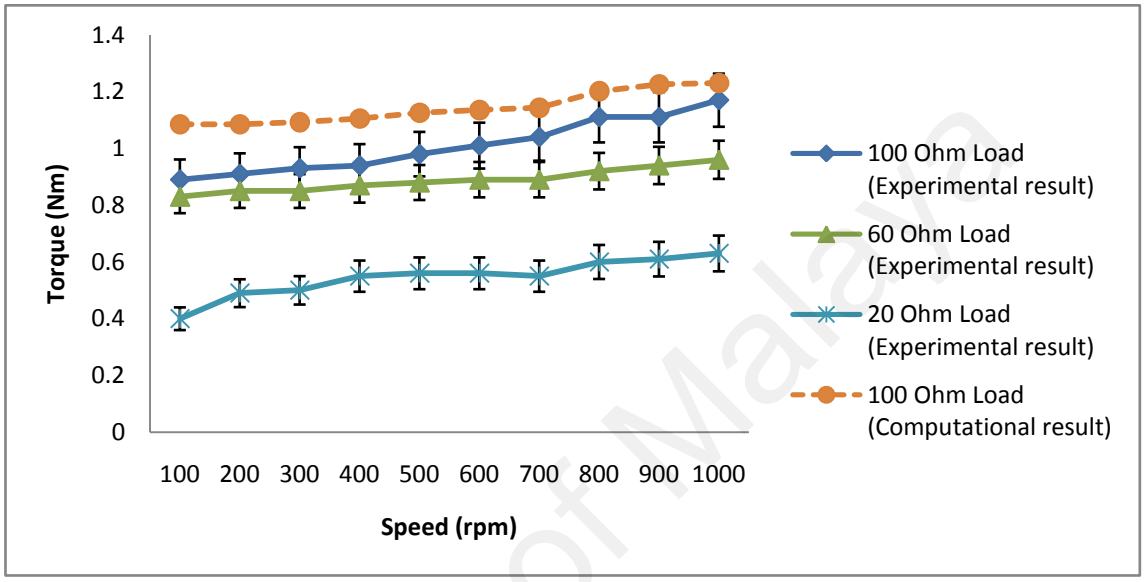

Figure 5.10: Torque versus speed.

5.4.4 Efficiency

Figures 5.11 and figure 5.12 show the graph of efficiency and temperature rise versus rotational speed. Figure 5.11 shows that machine efficiency versus speed with load resistance. It can be seen that the machine efficiency is proportional to the rotational speed as well as load resistance. The lowest efficiency obtained is 83% at 20 Ohm resistance while the highest recorded efficiency is 94% at 1000 rpm with resistance of 100 Ohm. For torque-efficiency characteristics, the machine efficiency increases from 10.7% to 94.8% with cogging torque of the 100 Ohm load is increased by 31.5%. It can be seen that the machine efficiency is proportional to the cogging torque. For instance, the measured efficiency has a maximum discrepancy of about 6% compared to the predicted efficiency at 100 Ohm load. The reason is when generator is

operating at lower speed, losses in the bearing-friction dominates the total losses. At high speed, major losses are attributed to the Eddy current losses in the windings (Wang & Kamper, 2004a).

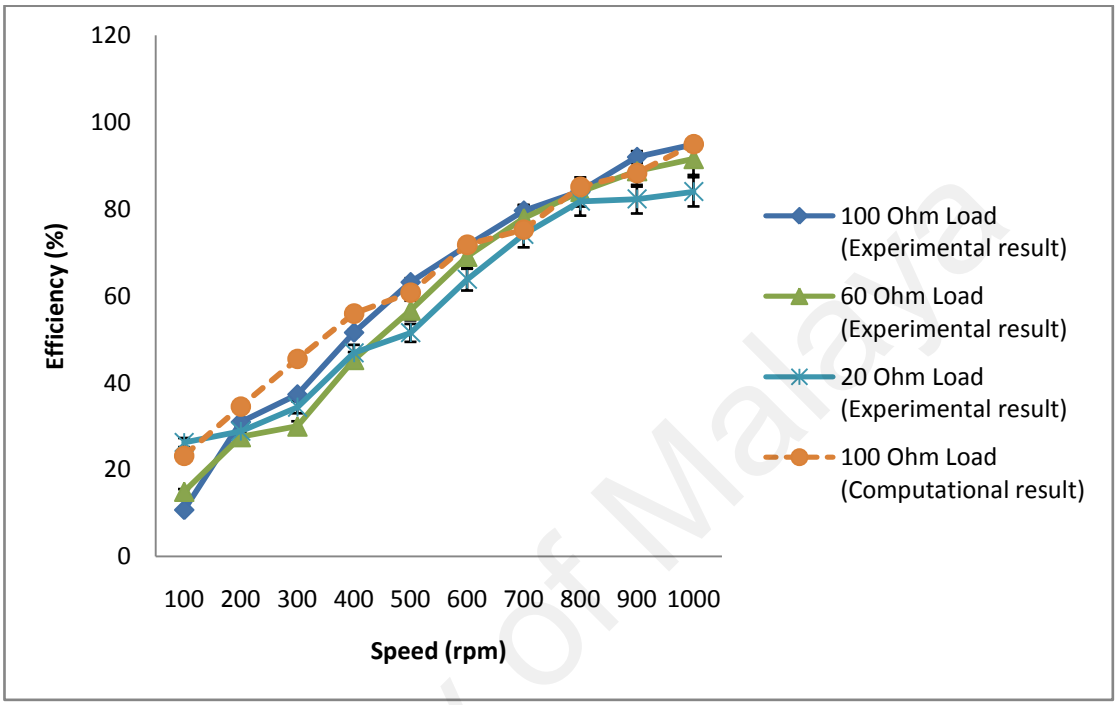

Figure 5.11: Efficiency versus speed.

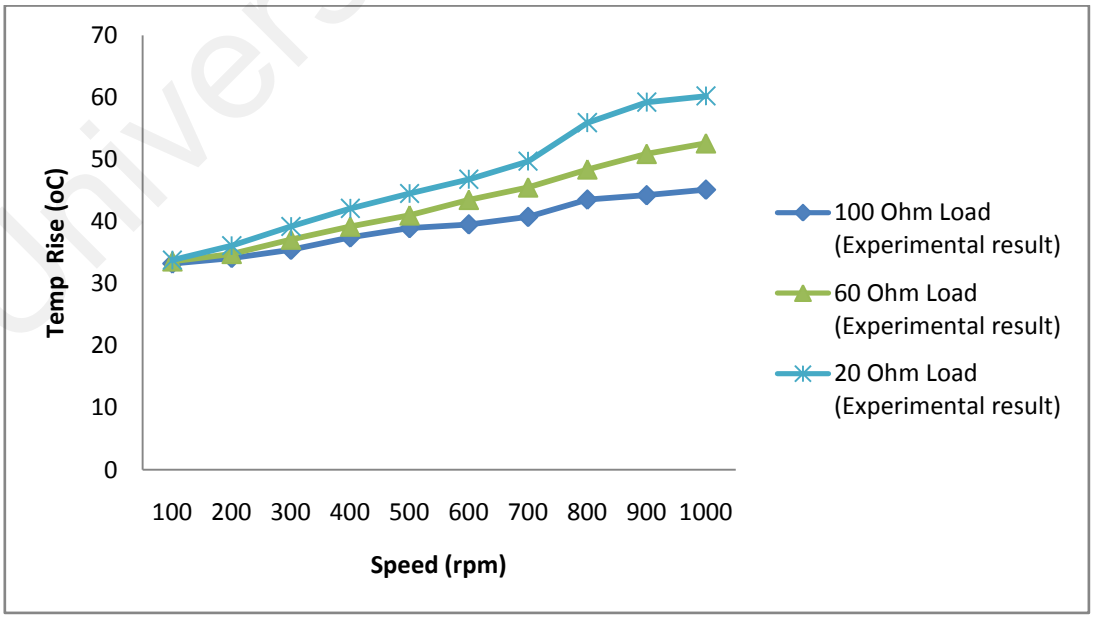

Figure 5.12: Temperature versus speed.

The stator windings temperature is obtained with an infrared thermometer. In figure 5.12, the graph shows the temperature rises linearly with rotational speed. At 20 Ohm load, the highest temperature recorded is around 61 Degree Celsius which is about twice higher than the ambient temperature in test lab. Therefore, the temperature is inversely proportional to load resistance due to losses in the form of heat in stator windings and this result corresponds to the output power characteristics of this generator.

Overall, the simulated efficiency is 95% and the measured efficiency is 94% at 1000 rpm. Because in a coreless electric machine with no core losses, the efficiency is higher than that of an iron-core machine which is normally less than 90% at relatively low speed (C. Chan et al., 1996; Guo, Zhu, Watterson, & Wu, 2003; Ali Mahmoudi et al., 2013). Both the experimental results and theoretical results are in good agreement.

CHAPTER 6: CONCLUSION

In this thesis, the main objective has been the design development of an axial-flux permanent magnet coreless generator based on an improved optimization method. The design tool presented incorporates a 3D-computation method and heuristic algorithm. The following are some of the derived conclusions;

- The optimized AFPM generator was built, tested and verified its` performance using comprehensive computer software and advanced test equipments.
- Sizing equations can be applied into designing an AFPM coreless generator that subject to multiple limitations and constraints. Certain parameters are controlled to obtain desired machine performance and characteristics.
- Hybrid GA-PS optimization model shows a better outcome in AFPM machine optimization particularly at lower population size. Hybrid GA-PS has obtained a very consistent fitness value even though with small population size.
- Eddy current losses in stator windings are less significant compared to bearing losses at high operation speed. A good less-friction bearing can improve machine performance.
- Non-ferromagnetic stator used in prototype AFPM coreless generator shows lower cogging torque compared to AFPM generator with iron-stator core.
- The double-sided AFPM generator has two air-gaps which is the space between outer surfaces of the permanent magnets and stator windings. In the prototype generator, the air-gap length is adjustable. It allows the investigation of the effect of air-gap on the prototype machine performance.
- Comparison for the efficiency in experiment with those obtained in FEA simulation show that the AFPM coreless generator could also achieve very high efficiency up

to 95%. Overall, both the experimental results and theoretical results are in good agreement.

REFERENCES

Acarnley, P.P., Mecrow, B.C., Burdess, J.S., Fawcett, J.N., Kelly, J.G., & Dickinson, P.G. (1996). Design Principles For A Flywheel Energy Store For Road Vehicles. *Ieee Transactions On Industry Applications, 32*(6), 1402-1408.

Açikbaş, S., & Söylemez, M. (2008). Coasting Point Optimisation For Mass Rail Transit Lines Using Artificial Neural Networks And Genetic Algorithms. *Iet Electric Power Applications, 2*(3), 172-182.

Amrita, M., & Mohan Rao, N. (2011). Optimal Design Of Multilayered Composite Plate Using Bio-Inspired Optimisation Techniques. *International Journal Of Bio-Inspired Computation, 3*(5), 306-319.

Atallah, K., Howe, D., Mellor, P.H., & Stone, D.A. (2000). Rotor Loss In Permanent-Magnet Brushless Ac Machines. *Ieee Transactions On Industry Applications, 36*(6), 1612-1618.

Aydin, M., Huang, S., & Lipo, T. (2004). Axial Flux Permanent Magnet Disc Machines: A Review. *Wisconsin Electric Machines & Power Electronics Consortium, University Of Wisconsin-Madison, Madison, Wi*, 53706-51691.

Aydin, M., Huang, S., & Lipo, T.A. (2006). Torque Quality And Comparison Of Internal And External Rotor Axial Flux Surface-Magnet Disc Machines. *Ieee Transactions On Industrial Electronics, 53*(3), 822-830.

Aydin, M., Zhu, Z., Lipo, T., & Howe, D. (2007). Minimization Of Cogging Torque In Axial-Flux Permanent-Magnet Machines: Design Concepts. *Magnetics, Ieee Transactions On, 43*(9), 3614-3622.

Azzouzi, J., Barakat, G., & Dakyo, B. (2005). Quasi-3-D Analytical Modeling Of The Magnetic Field Of An Axial Flux Permanent-Magnet Synchronous Machine. *Energy Conversion, Ieee Transactions On, 20*(4), 746-752.

Baptista, S.S., Kothandaraman, A., & Vijay, S. (2010). Axial Flux Permanent Magnet Generator. *Artificial Intelligent Systems And Machine Learning, 2*(12).

Barakat, G., El-Meslouhi, T., & Dakyo, B. (2001). Analysis Of The Cogging Torque Behavior Of A Two-Phase Axial Flux Permanent Magnet Synchronous Machine. *Ieee Transactions On Magnetics, 37*(4), 2803-2805.

Binns, K. (1964). Calculation Of Some Basic Flux Quantities In Induction And Other Doubly-Slotted Electrical Machines. *Electrical Engineers, Proceedings Of The Institution Of, 111*(11), 1847-1858.

Bumby, J., & Martin, R. (2005). Axial-Flux Permanent-Magnet Air-Cored Generator For Small-Scale Wind Turbines. *Iee Proceedings-Electric Power Applications, 152*(5), 1065-1075.

Bumby, J., Martin, R., Mueller, M., Spooner, E., Brown, N., & Chalmers, B. (2004). Electromagnetic Design Of Axial-Flux Permanent Magnet Machines. *Iee Proceedings-Electric Power Applications, 151*(2), 151-160.

Căleanu, C.-D., Mao, X., Pradel, G., Moga, S., & Xue, Y. (2011). Combined Pattern Search Optimization Of Feature Extraction And Classification Parameters In Facial Recognition. *Pattern Recognition Letters, 32*(9), 1250-1255.

Campbell, P. (1974). Principles Of A Permanent-Magnet Axial-Field Dc Machine. *Electrical Engineers, Proceedings Of The Institution Of, 121*(12), 1489-1494.

Campbell, P. (1975). The Magnetic Circuit Of An Axial Field Dc Electrical Machine. *Magnetics, Ieee Transactions On, 11*(5), 1541-1543.

Cao, Y., & Wu, Q. (1999). Teaching Genetic Algorithm Using Matlab. *International Journal Of Electrical Engineering Education, 36*(2), 139-153.

Caricchi, F., Crescimbini, F., & Honorati, O. (1998). Low-Cost Compact Permanent Magnet Machine For Adjustable-Speed Pump Application. *Ieee Transactions On Industry Applications, 34*(1), 109-116.

Caricchi, F., Crescimbini, F., Honorati, O., Di Napoli, A., & Santini, E. (1996). Compact Wheel Direct Drive For Evs. *Ieee Industry Applications Magazine, 2*(6), 25-32.

Caricchi, F., Crescimbini, F., & Santini, E. (1995). Basic Principle And Design Criteria Of Axial-Flux Pm Machines Having Counterrotating Rotors. *Ieee Transactions On Industry Applications, 31*(5), 1062-1068.

Chalmers, B., & Spooner, E. (1999). An Axial-Flux Permanent-Magnet Generator For A Gearless Wind Energy System. *Energy Conversion, Ieee Transactions On, 14*(2), 251-257.

Chan, C., Chau, K., Jiang, J., Xia, W., Zhu, M., & Zhang, R. (1996). Novel Permanent Magnet Motor Drives For Electric Vehicles. *Ieee Transactions On Industrial Electronics, 43*(2), 331-339.

Chan, C.C. (1987). Axial-Field Electrical Machines-Design And Applications. *Energy Conversion, Ieee Transactions On*(2), 294-300.

Chan, T., & Lai, L. (2007). An Axial-Flux Permanent-Magnet Synchronous Generator For A Direct-Coupled Wind-Turbine System. *Ieee Transactions On Energy Conversion, 22*(1), 86-94.

Chen, Y., Pillay, P., & Khan, A. (2005). Pm Wind Generator Topologies. *Ieee Transactions On Industry Applications, 41*(6), 1619-1626.

Choi, J.-Y., Lee, S.-H., Ko, K.-J., & Jang, S.-M. (2011). Improved Analytical Model For Electromagnetic Analysis Of Axial Flux Machines With Double-Sided Permanent Magnet Rotor And Coreless Stator Windings. *Ieee Transactions On Magnetics, 47*(10), 2760-2763.

Chung, D.-W., & You, Y.-M. (2014). Design And Performance Analysis Of Coreless Axial-Flux Permanent-Magnet Generator For Small Wind Turbines. *Journal Of Magnetics, 19*(3), 273-281.

Coello Coello, C.A., & Christiansen, A.D. (1999). Moses: A Multiobjective Optimization Tool For Engineering Design. *Engineering Optimization, 31*(3), 337-368.

Dao, S.D., Abhary, K., & Marian, R. (2016). Maximising Performance Of Genetic Algorithm Solver In Matlab. *Eng. Lett, 24*(1), 75-83.

De La Barriere, O., Hlioui, S., Ben Ahmed, H., Gabsi, M., & Lobue, M. (2012). 3-D Formal Resolution Of Maxwell Equations For The Computation Of The No-Load Flux In An Axial Flux Permanent-Magnet Synchronous Machine. *Magnetics, Ieee Transactions On, 48*(1), 128-136.

Demenko, A. (1996). Movement Simulation In Finite Element Analysis Of Electric Machine Dynamics. *Ieee Transactions On Magnetics, 32*(3), 1553-1556.

Di Stefano, R., & Marignetti, F. (2012). Electromagnetic Analysis Of Axial-Flux Permanent Magnet Synchronous Machines With Fractional Windings With Experimental Validation. *Ieee Transactions On Industrial Electronics, 59*(6), 2573-2582.

Duan, Y., & Ionel, D.M. (2013). A Review Of Recent Developments In Electrical Machine Design Optimization Methods With A Permanent-Magnet Synchronous Motor Benchmark Study. *Ieee Transactions On Industry Applications, 49*(3), 1268-1275.

Dubois, M., Polinder, H., & Ferreira, J. (2000). Comparison Of Generator Topologies For Direct-Drive Wind Turbines. *Proceedings Of Norpie'00*, 22-26.

Eastham, J.F., Profumo, F., Tenconi, A., Hill-Cottingham, R., Coles, P., & Gianolio, G. (2002). Novel Axial Flux Machine For Aircraft Drive: Design And Modeling. *Ieee Transactions On Magnetics, 38*(5), 3003-3005.

El Shahat, A., Keyhani, A., & El Shewy, H. (2010). Sizing A High Speed Pm Generator For Green Energy Applications. *Journal Of Electrical Systems, 6*, 16.

Fei, W., Luk, P.C.-K., & Jinupun, K. (2010). Design And Analysis Of High-Speed Coreless Axial Flux Permanent Magnet Generator With Circular Magnets And Coils. *Iet Electric Power Applications, 4*(9), 739-747.

Gholamian, S., Ardebil, M., Abbaszadeh, K., & Charati, S.M. (2005). Optimum Design Of 1kw Axial Flux Permanent Magnet Slotted Torus Motor. *Editorial Advisory Board E, 21*(3), 488-499.

Gholamian, S.A., Ablouie, M.A., Mohseni, A., & Jafarabadi, S.E. (2009). Effect Of Air Gap On Torque Density For Double-Sided Axial Flux Slotted Permanent Magnet Motors Using Analytic And Fem Evaluation. *Journal Of Applied Sciences Research, 5*(9), 1230-1238.

Güneş, F., & Tokan, F. (2011). Amplitude-Only Pattern Synthesis Of Nonuniform Linear Arrays Using A Generalized Pattern Search Optimization. *International Journal Of Rf And Microwave Computer-Aided Engineering, 21*(3), 251-262.

Guo, Y., Zhu, J.G., Watterson, P.A., & Wu, W. (2003). Comparative Study Of 3-D Flux Electrical Machines With Soft Magnetic Composite Cores. *Ieee Transactions On Industry Applications, 39*(6), 1696-1703.

Hesse, M.H. (1992). Air Gap Permeance In Doubly-Slotted Asynchronous Machines. *Ieee Transactions On Energy Conversion, 7*(3), 491-499.

Hosseini, S., Agha-Mirsalim, M., & Mirzaei, M. (2008). Design, Prototyping And Analysis Of A Low-Cost Disk Permanent Magnet Generator With Rectangular Flat-Shaped Magnets. *Iranian Journal Of Science And Technology, 32*(B), 191.

Huang, S., Luo, J., Leonardi, F., & Lipo, T. (1997). A Comparison Of Power Density For Axial Flux Machines Based On General Purpose Sizing Equations. *Ieee Power Engineering Review, 17*(11), 55.

Huang, S., Luo, J., Leonardi, F., & Lipo, T. (1998). A General Approach To Sizing And Power Density Equations For Comparison Of Electrical Machines. *Industry Applications, Ieee Transactions On, 34*(1), 92-97.

Hüner, E., & Aküner, C. (2012). Axial-Flux Synchronous Machines Compared With Different Stator Structures For Use In Working. *Przegląd Elektrotechniczny Selected Full Texts, 88*(11a), 174-177.

Hwang, C.-C., Li, P.-L., Chuang, F.C., Liu, C.-T., & Huang, K.-H. (2009). Optimization For Reduction Of Torque Ripple In An Axial Flux Permanent Magnet Machine. *Ieee Transactions On Magnetics, 45*(3), 1760-1763.

Islam, M.S., Islam, R., Sebastian, T., Chandy, A., & Ozsoylu, S.A. (2011). Cogging Torque Minimization In Pm Motors Using Robust Design Approach. *Ieee Transactions On Industry Applications, 47*(4), 1661-1669.

Jahns, T.M., & Soong, W.L. (1996). Pulsating Torque Minimization Techniques For Permanent Magnet Ac Motor Drives-A Review. *Ieee Transactions On Industrial Electronics, 43*(2), 321-330.

Javadi, S., & Mirsalim, M. (2010). Design And Analysis Of 42-V Coreless Axial-Flux Permanent-Magnet Generators For Automotive Applications. *Magnetics, Ieee Transactions On, 46*(4), 1015-1023.

Jiang, W., & Jahns, T.M. (2015). Coupled Electromagnetic–Thermal Analysis Of Electric Machines Including Transient Operation Based On Finite-Element Techniques. *Ieee Transactions On Industry Applications, 51*(2), 1880-1889.

Juang, C.-F. (2004). A Hybrid Of Genetic Algorithm And Particle Swarm Optimization For Recurrent Network Design. *Ieee Transactions On Systems, Man, And Cybernetics, Part B (Cybernetics), 34*(2), 997-1006.

Jung, T.-U., & Cho, J.-S. (2011). Electromagnetic Structural Design Analysis And Performance Improvement Of Afpm Generator For Small Wind Turbine. *Journal Of Magnetics, 16*(4), 374-378.

Kahourzade, S., Mahmoudi, A., Ping, H.W., & Uddin, M.N. (2014). A Comprehensive Review Of Axial-Flux Permanent-Magnet Machines. *Canadian Journal Of Electrical And Computer Engineering, 37*(1), 19-33.

Kao, Y.-T., & Zahara, E. (2008). A Hybrid Genetic Algorithm And Particle Swarm Optimization For Multimodal Functions. *Applied Soft Computing, 8*(2), 849-857.

Kim, J.-K., Cho, D.-H., Jung, H.-K., & Lee, C.-G. (2002). Niching Genetic Algorithm Adopting Restricted Competition Selection Combined With Pattern Search Method. *Ieee Transactions On Magnetics, 38*(2), 1001-1004.

Kim, J., & Kasabov, N. (1999). Hyfis: Adaptive Neuro-Fuzzy Inference Systems And Their Application To Nonlinear Dynamical Systems. *Neural Networks, 12*(9), 1301-1319.

Kuo, E., & Wieman, C.E. (2016). Toward Instructional Design Principles: Inducing Faraday's Law With Contrasting Cases. *Physical Review Physics Education Research, 12*(1), 010128.

Kurronen, P., & Pyrhönen, J. (2007). Analytic Calculation Of Axial-Flux Permanent-Magnet Motor Torque. *Electric Power Applications, Iet, 1*(1), 59-63.

Lee, J.K. (1992). Measurement Of Magnetic Fields In Axial Field Motors. *Magnetics, Ieee Transactions On, 28*(5), 3021-3023.

Lee, K.S., & Geem, Z.W. (2005). A New Meta-Heuristic Algorithm For Continuous Engineering Optimization: Harmony Search Theory And Practice. *Computer Methods In Applied Mechanics And Engineering, 194*(36), 3902-3933.

Leung, W.S., & Chan, J.C. (1980). A New Design Approach For Axial-Field Electrical Machines. *Power Apparatus And Systems, Ieee Transactions On*(4), 1679-1685.

Li, H., & Chen, Z. (2008). Overview Of Different Wind Generator Systems And Their Comparisons. *Iet Renewable Power Generation, 2*(2), 123-138.

Locment, F., Semail, E., & Piriou, F. (2006). Design And Study Of A Multiphase Axial-Flux Machine. *Magnetics, Ieee Transactions On, 42*(4), 1427-1430.

Lombard, N., & Kamper, M. (1999). Analysis And Performance Of An Ironless Stator Axial Flux Pm Machine. *Energy Conversion, Ieee Transactions On, 14*(4), 1051-1056.

Mahmoudi, A., Kahourzade, S., Rahim, N.A., & Hew, W.P. (2013). Design, Analysis, And Prototyping Of An Axial-Flux Permanent Magnet Motor Based On Genetic Algorithm And Finite-Element Analysis. *Magnetics, Ieee Transactions On, 49*(4), 1479-1492.

Mahmoudi, A., Kahourzade, S., Rahim, N.A., Ping, H.W., & Uddin, M.N. (2013). Design And Prototyping Of An Optimised Axial-Flux Permanent-Magnet Synchronous Machine. *Iet Electric Power Applications, 7*(5), 338-349.

Mahmoudi, A., Rahim, N., & Hew, W. (2011). Torus And Afir Axial-Flux Permanent-Magnet Machines: A Comparison Via Finite Element Analysis. *International Review On Modelling And Simulations, 4*(2).

Marignetti, F., Colli, V.D., & Carbone, S. (2010). Comparison Of Axial Flux Pm Synchronous Machines With Different Rotor Back Cores. *Ieee Transactions On Magnetics, 46*(2), 598-601.

Marignetti, F., Colli, V.D., & Coia, Y. (2008). Design Of Axial Flux Pm Synchronous Machines Through 3-D Coupled Electromagnetic Thermal And Fluid-Dynamical Finite-Element Analysis. *Industrial Electronics, Ieee Transactions On, 55*(10), 3591-3601.

Marinakis, Y., Marinaki, M., & Dounias, G. (2010). A Hybrid Particle Swarm Optimization Algorithm For The Vehicle Routing Problem. *Engineering Applications Of Artificial Intelligence, 23*(4), 463-472.

Mirzaeian, B., Moallem, M., Tahani, V., & Lucas, C. (2002). Multiobjective Optimization Method Based On A Genetic Algorithm For Switched Reluctance Motor Design. *Ieee Transactions On Magnetics, 38*(3), 1524-1527.

Montazeri-Gh, M., Poursamad, A., & Ghalichi, B. (2006). Application Of Genetic Algorithm For Optimization Of Control Strategy In Parallel Hybrid Electric Vehicles. *Journal Of The Franklin Institute, 343*(4), 420-435.

Mueller, M.A., & Mcdonald, A.S. (2009). A Lightweight Low-Speed Permanent Magnet Electrical Generator For Direct-Drive Wind Turbines. *Wind Energy, 12*(8), 768-780.

Muljadi, E., Butterfield, C.P., & Wan, Y.-H. (1999a). Axial-Flux Modular Permanent-Magnet Generator With A Toroidal Winding For Wind-Turbine Applications. *Industry Applications, Ieee Transactions On, 35*(4), 831-836.

Muljadi, E., Butterfield, C.P., & Wan, Y.-H. (1999b). Axial-Flux Modular Permanent-Magnet Generator With A Toroidal Winding For Wind-Turbine Applications. *Ieee Transactions On Industry Applications, 35*(4), 831-836.

Nédélec, J.-C. (1980). Mixed Finite Elements In ℝ3. *Numerische Mathematik, 35*(3), 315-341.

Nguyen, T.D., Tseng, K.-J., Zhang, S., & Nguyen, H.T. (2011). A Novel Axial Flux Permanent-Magnet Machine For Flywheel Energy Storage System: Design And Analysis. *Ieee Transactions On Industrial Electronics, 58*(9), 3784-3794.

Niazi, P., Toliyat, H.A., Cheong, D.-H., & Kim, J.-C. (2007). A Low-Cost And Efficient Permanent-Magnet-Assisted Synchronous Reluctance Motor Drive. *Ieee Transactions On Industry Applications, 43*(2), 542-550.

Oh, S.C., & Emadi, A. (2004). Test And Simulation Of Axial Flux-Motor Characteristics For Hybrid Electric Vehicles. *Ieee Transactions On Vehicular Technology, 53*(3), 912-919.

Park, Y.-S., Koo, M.-M., Jang, S.-M., Choi, J.-Y., & You, D.-J. (2015). Performance Evaluation Of Radial-And Axial-Flux Pm Wind Power Generators With Mechanical Energy Storage System. *Ieee Transactions On Energy Conversion, 30*(1), 237-245.

Parviainen, A., Niemela, M., & Pyrhonen, J. (2004). Modeling Of Axial Flux Permanent-Magnet Machines. *Ieee Transactions On Industry Applications, 40*(5), 1333-1340.

Platt, D. (1989). Permanent Magnet Synchronous Motor With Axial Flux Geometry. *Magnetics, Ieee Transactions On, 25*(4), 3076-3079.

Profumo, F., Zhang, Z., & Tenconi, A. (1997). Axial Flux Machines Drives: A New Viable Solution For Electric Cars. *Ieee Transactions On Industrial Electronics, 44*(1), 39-45.

Pullen, K., Etemad, M., & Fenocchi, A. (1996). The High Speed Axial Flux Disc Generator-Unlocking The Potential Of The Automotive Gas Turbine. *Iee Colloquium On Machines And Drives For Electric And Hybrid Vehicles, 1*(8).

Qu, R., & Lipo, T.A. (2003). Dual-Rotor, Radial-Flux, Toroidally Wound, Permanent-Magnet Machines. *Ieee Transactions On Industry Applications, 39*(6), 1665-1673.

Raajan, M.V., Bharanikumar, R., Bhuvaneswari, S., & Subramanian, C. (2015). Design And Optimisation Of Permanent Magnet Synchronous Generator For Wind-Turbine Applications. *International Journal Of Research And Innovation In Engineering Technology, 1*(12).

Rahman, M.A., & Zhou, P. (1996). Analysis Of Brushless Permanent Magnet Synchronous Motors. *Ieee Transactions On Industrial Electronics, 43*(2), 256-267.

Rashtchi, V., Rahimpour, E., & Fotoohabadi, H. (2011). Parameter Identification Of Transformer Detailed Model Based On Chaos Optimisation Algorithm. *Iet Electric Power Applications, 5*(2), 238-246.

Rostami, N., Feyzi, M.R., Pyrhönen, J., Parviainen, A., & Behjat, V. (2012). Genetic Algorithm Approach For Improved Design Of A Variable Speed Axial-Flux Permanent-Magnet Synchronous Generator. *Magnetics, Ieee Transactions On, 48*(12), 4860-4865.

Rovio, T., Vihriälä, H., Söderlund, L., Kriikka, J., & Hyppönen, M. (2001). Axial And Radial Flux Generators In Small-Scale Wind Power Production. *Energy (Kwh), 30*, 40.

Sadeghierad, M., Darabi, A., Lesani, H., & Monsef, H. (2010). Optimal Design Of The Generator Of Microturbine Using Genetic Algorithm And Pso. *International Journal Of Electrical Power & Energy Systems, 32*(7), 804-808.

Sadeghierad, M., Lesani, H., Monsef, H., & Darabi, A. (2009a). High-Speed Axial-Flux Permanent-Magnet Generator With Coreless Stator. *Electrical And Computer Engineering, Canadian Journal Of, 34*(1/2), 63-67.

Sadeghierad, M., Lesani, H., Monsef, H., & Darabi, A. (2009b). High-Speed Axial-Flux Permanent-Magnet Generator With Coreless Stator. *Canadian Journal Of Electrical And Computer Engineering, 34*(1/2), 63-67.

Santiago, J., & Bernhoff, H. (2010). Regular Paper Comparison Between Axial And Radial Flux Pm Coreless Machines For Flywheel Energy Storage. *J. Electrical Systems, 6*, 2.

Schwarz, K. (1991). Ac Machines: Electromagnetics And Design. *Power Engineering Journal, 5*(5), 248-248.

Sharma, P., Bhatti, T., & Ramakrishnan, K. (2011). Permanent-Magnet Induction Generators: An Overview. *Journal Of Engineering Science And Technology, 6*(3), 332-338.

Söderlund, L., Eriksson, J., Salonen, J., Vihriälä, H., & Perälä, R. (1996). A Permanent-Magnet Generator For Wind Power Applications. *Ieee Transactions On Magnetics, 32*(Conf-950691--).

Spooner, E., & Chalmers, B. (1992). Torus': A Slotless, Toroidal-Stator, Permanent-Magnet Generator. *The Iee Proceedings B-Electric Power Applications*. *139*(6), 497-506.

Takano, H., Itoh, T., Mori, K., Sakuta, A., & Hirasa, T. (1992). Optimum Values For Magnet And Armature Winding Thickness For Axial-Field Permanent Magnet Brushless Dc Motors. *Industry Applications, Ieee Transactions On, 28*(2), 350-357.

Upadhyay, P.R., & Rajagopal, K. (2006). Fe Analysis And Computer-Aided Design Of A Sandwiched Axial-Flux Permanent Magnet Brushless Dc Motor. *Magnetics, Ieee Transactions On, 42*(10), 3401-3403.

Virtič, P., & Avsec, J. (2011). Analysis Of Coreless Stator Axial Flux Permanent Magnet Synchronous Generator Characteristics By Using Equivalent Circuit. *Przeglad Elektrotechniczny, 87*(3), 208-211.

Wang, R.-J., & Kamper, M.J. (2004a). Calculation Of Eddy Current Loss In Axial Field Permanent-Magnet Machine With Coreless Stator. *Ieee Transactions On Energy Conversion, 19*(3), 532-538.

Wang, R.-J., & Kamper, M.J. (2004b). Calculation Of Eddy Current Loss In Axial Field Permanent-Magnet Machine With Coreless Stator. *Energy Conversion, Ieee Transactions On, 19*(3), 532-538.

Wang, R.-J., Kamper, M.J., Van Der Westhuizen, K., & Gieras, J.F. (2005). Optimal Design Of A Coreless Stator Axial Flux Permanent-Magnet Generator. *Ieee Transactions On Magnetics, 41*(1), 55-64.

Xu, Y., Zeng, M., Liu, Q., & Wang, X. (2014). A Genetic Algorithm Based Multilevel Association Rules Mining For Big Datasets. *Mathematical Problems In Engineering, 2014*.

Zhilichev, Y.N. (1998). Three-Dimensional Analytic Model Of Permanent Magnet Axial Flux Machine. *Ieee Transactions On Magnetics, 34*(6).

LIST OF PUBLICATIONS AND PAPERS PRESENTED

List of Publications

Lok, C.L., Vengadaesvaran, B., & Ramesh, S. (2016). Implementation Of Hybrid Pattern Search–Genetic Algorithm Into Optimizing Axial-Flux Permanent Magnet Coreless Generator (Afpmg). *Electrical Engineering*, 1-11.

List of Conferences

Lok, C.L., Vengadaesvaran, B., & Ramesh, S. (2015). An Experimental Study And Optimization Of Axial-Flux Permanent Magnet Coreless Generator For Delayed Pulse Generation. Poster Presented At The 5th International Conference On Functional Materials And Devices (Icfmd 2015), Johor, Malaysia.